Evolution of Avian Plumage Color in a Tetrahedral Color Space: A Phylogenetic Analysis of New World Buntings

Mary Caswell Stoddard and Richard O. Prum*

Department of Ecology and Evolutionary Biology and the Peabody Museum of Natural History, Yale University, New Haven, Connecticut 06511

Submitted June 1, 2007; Accepted January 18, 2008; Electronically published April 14, 2008

Online enhancement: appendix.

ABSTRACT: We use a tetrahedral color space to describe and analyze male plumage color variation and evolution in a clade of New World buntings—*Cyanocompsa* and *Passerina* (Aves: Cardinalidae). The Goldsmith color space models the relative stimulation of the four retinal cones, using the integrals of the product of plumage reflectance spectra and cone sensitivity functions. A color is represented as a vector defined by the relative stimulation of the four cone types—ultraviolet, blue, green, and red. Color vectors are plotted in a tetrahedral, or quaternary, plot with the achromatic point at the origin and the ultraviolet/violet channel along the *Z*-axis. Each color vector is specified by the spherical coordinates θ, ϕ, and r. Hue is given by the angles θ and ϕ. Chroma is given by the magnitude of r, the distance from the achromatic origin. Color vectors of all distinct patches in a plumage characterize the plumage color phenotype. We describe the variation in color space occupancy of male bunting plumages, using various measures of color contrast, hue contrast and diversity, and chroma. Comparative phylogenetic analyses using linear parsimony (in MacClade) and generalized least squares (GLS) models (in CONTINUOUS) with a molecular phylogeny of the group document that plumage color evolution in the clade has been very dynamic. The single best-fit GLS evolutionary model of plumage color variation over the entire clade is a directional change model with no phylogenetic correlation among species. However, phylogenetic innovations in feather color production mechanisms—derived pheomelanin and carotenoid expression in two lineages—created new opportunities to colonize novel areas of color space and fostered the explosive differentiation in plumage color. Comparison of the tetrahedral color space of Goldsmith with that of Endler and Mielke demonstrates that both provide essentially identical results. Evolution of avian ultraviolet/violet opsin sensitivity in relation to chromatic experience is discussed.

Keywords: *Passerina*, *Cyanocompsa*, hue, chroma, color vision, ultraviolet.

* E-mail: richard.prum@yale.edu.

Am. Nat. 2008. Vol. 171, pp. 000–000.
0003-0147/2008/17106-42642$15.00.
DOI: 10.1086/587526

Plumage color plays an important role in communication and social signaling of birds (Hill and McGraw 2006*b*). However, biologists have only recently begun to understand how the complexity of visual perception of birds has contributed to evolution of plumage coloration (Cuthill et al. 1999; Hart 2001; Eaton and Lanyon 2003; Eaton 2005; Endler and Mielke 2005). Inadequate appreciation of the complexity of avian color vision and the lack of well-supported avian phylogenies have hindered our ability to explore quantitatively the evolution of avian plumage color in a historical context.

Burkhardt (1989) and Goldsmith (1990) first proposed tetrahedral avian color spaces in which any perceived color can be described as a point in a tetrahedron determined by the relative stimulation of the four retinal cone types (fig. 1). The four vertices of the tetrahedron correspond to the ultraviolet- or violet-sensitive (UVS or VS), short-wavelength-sensitive or blue (SWS), medium-wavelength-sensitive or green (MWS), and long-wavelength-sensitive or red (LWS) cone photoreceptors. Each color has a unique set of relative stimulation values, {*u/v s m l*}, and a unique position in the color space.

Despite early theoretical suggestions by Burkhardt (1989) and Goldsmith (1990), tetrachromatic color spaces have rarely been used in analyses of avian color (e.g., Vorobyev et al. 1998). Recently, however, Endler and Mielke (2005) described a tetrahedral avian color vision space in which they explicitly attempt to model the sensory experience of the visual signal receiver. Based on physiological models of avian color vision, Endler and Mielke's (2005) method incorporates ambient light spectra, background reflectance, environmental transmission, ocular transmission, oil droplet absorbance, and cone pigment absorbance of the species and environments being mod-

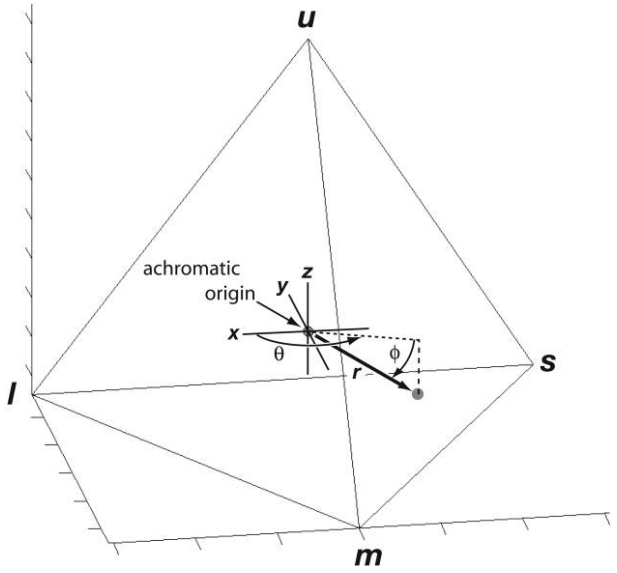

Figure 1: A tetrahedral color space. Each color is a point in the tetrahedron determined by the relative stimulation of the four cone color channels—*u* (or *v*), *s*, *m*, and *l*. The achromatic point of equivalent stimulation of all channels is at the origin, and the ultraviolet or violet channel, *u* or *v*, is along the *Z*-axis (Endler and Mielke 2005). Each color can be described by a vector with the spherical coordinates θ, ϕ, and *r*. Angle θ is the horizontal, azimuth angle from the positive *X*-axis to the color vector. Angle ϕ is the vertical, elevation angle from the *X*-*Y* plane to the color vector. θ and ϕ are analogous to longitude and latitude, respectively. The length of the color vector is given by *r*. Together, θ and ϕ describe the hue, or the direction, of the color vector, and *r* is a measure of chroma, or saturation, which describes how different a color is from achromatic white/black.

eled. Endler et al. (2005) used this vision space in an analysis of bowerbird plumage and bower ornamentation.

The variation and distribution of colors plotted in a tetrahedral color space can be used to study avian plumage color patterns. Endler and Mielke (2005) proposed measures of plumage color contrast in the color space and developed a statistical method to test for significant differences between the spatial distributions of two color patterns in color space.

Here, we apply the tetrahedral color space of Goldsmith (1990) to analyze avian reflectance spectra directly, controlling for variation in sensory environment. We map reflectance spectra directly into a tetrahedral color space based on the stimulation of the four avian cone types by the reflectance spectrum under idealized illumination. In contrast, Endler and colleagues (Endler and Mielke 2005; Endler et al. 2005) incorporated ambient light variation to model the sensory experience of the signal receiver. Despite the justified enthusiasm for tetrachromatic analysis of the realized signal, or receiver sensory phenotype (Endler and Mielke 2005; Endler et al. 2005), it is also important to develop and employ tools for the tetrachromatic analysis of variation and evolution of the signaler phenotype (i.e., avian reflectance spectra themselves), independent of environmental conditions. Understanding visual communication requires mapping the signaler phenotype onto the realized sensory phenotype of the receiver in a given sensory environment. Accordingly, we compare the color spaces of Goldsmith (1990) and Endler and Mielke (2005), using New World bunting plumages.

Phylogenetic Natural History of Color Evolution in a Clade

The primary goal of our analysis of male plumage coloration in a clade of New World buntings and grosbeaks—*Cyanocompsa* and *Passerina* (Cardinalidae; fig. 2)—is to produce a phylogenetic natural history of plumage color evolution and color space occupancy in a clade. The 10 species of *Cyanocompsa* and *Passerina* buntings have diverse and varied plumage colors and patterns (fig. 2). Their plumages incorporate a wide range of colors, including white, black, ultraviolet, violet, blue, turquoise, green, yellow, UV-yellow, orange, brown, pink, red, and UV-red hues (figs. 2, 3). These plumage colors are produced by a broad variety of physical mechanisms, including pigments, structural colors, and combinations of both.

We measured the reflectance spectra of plumage patches of males of all species of *Cyanocompsa* and *Passerina* buntings and projected these colors into a tetrahedral color space (following Goldsmith [1990]). Next, we characterized the color space occupancy of each species, using various measures developed by Endler and Mielke (2005) and new measures proposed here (e.g., hue disparity, achieved chroma). We then examined phylogenetic patterns in the evolution of plumage color using a molecular phylogeny of the *Cyanocompsa-Passerina* clade by Klicka et al. (2001). First, we employed the linear parsimony algorithm in MacClade (Maddison and Maddison 2000), and then we used the generalized least squares method implemented in the computer program CONTINUOUS (Pagel 1997, 1999) to examine alternative quantitative models of the evolution of plumage color measures over the phylogeny. In addition, we present quantitative expressions for the relationship between relative cone stimulation and chroma for a given hue (see "Function of Cone Stimulation for a Given Hue" in the appendix in the online edition of the *American Naturalist*), the maximum chroma for any hue (see "Maximum Chroma" in the appendix in the online edition of the *American Naturalist*), and the variation in maximum chroma for hues across the visible spectrum for the UV and violet cone–type avian visual systems (see "Discussion").

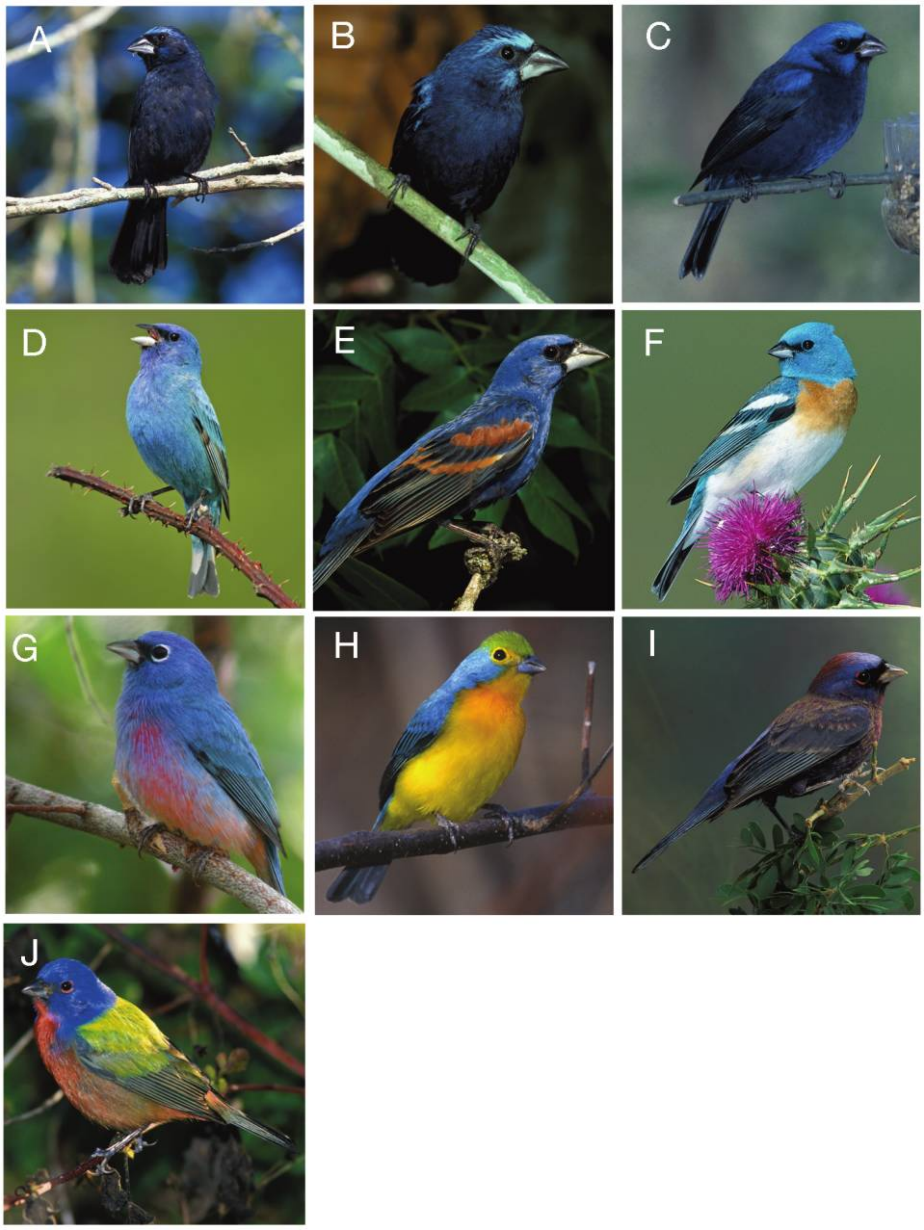

Figure 2: Adult male plumages of *Cyanocompsa* and *Passerina* buntings (Cardinalidae). *A*, Ultramarine grosbeak *Cyanocompsa brissonii*; *B*, blue-black grosbeak *Cyanocompsa cyanoides*; *C*, blue bunting *Cyanocompsa parellina*; *D*, indigo bunting *Passerina cyanea*; *E*, blue grosbeak *Passerina caerulea*; *F*, lazuli bunting *Passerina amoena*; *G*, Rosita's bunting *Passerina rositae*; *H*, orange-breasted bunting *Passerina leclancherii*; *I*, varied bunting *Passerina versicolor*; *J*, painted bunting *Passerina ciris*. Photo credits: *A*, E. Endrigo, Visual Resources for Ornithology (VIREO); *B*, D. Wechsler, VIREO; *C*, *J*, J. Culbertson, VIREO; *D*, G. McElroy, VIREO; *E*, *I*, R. and N. Bowers, VIREO; *F*, P. LaTourette; *G*, M. Grosselet and G. Ruiz; *H*, J. Ownby.

Methods

The methods are presented here in abbreviated form. A full description of all methods is presented in "Detailed Methods" in the appendix in the online edition of the *American Naturalist*.

Plumage Color Measurement

We measured the reflectance spectra of 10 plumage patches of 10 males of all species in the cardinalid genera *Cyanocompsa* (three species) and *Passerina* (seven species). The clade was selected because of its rich and varied color

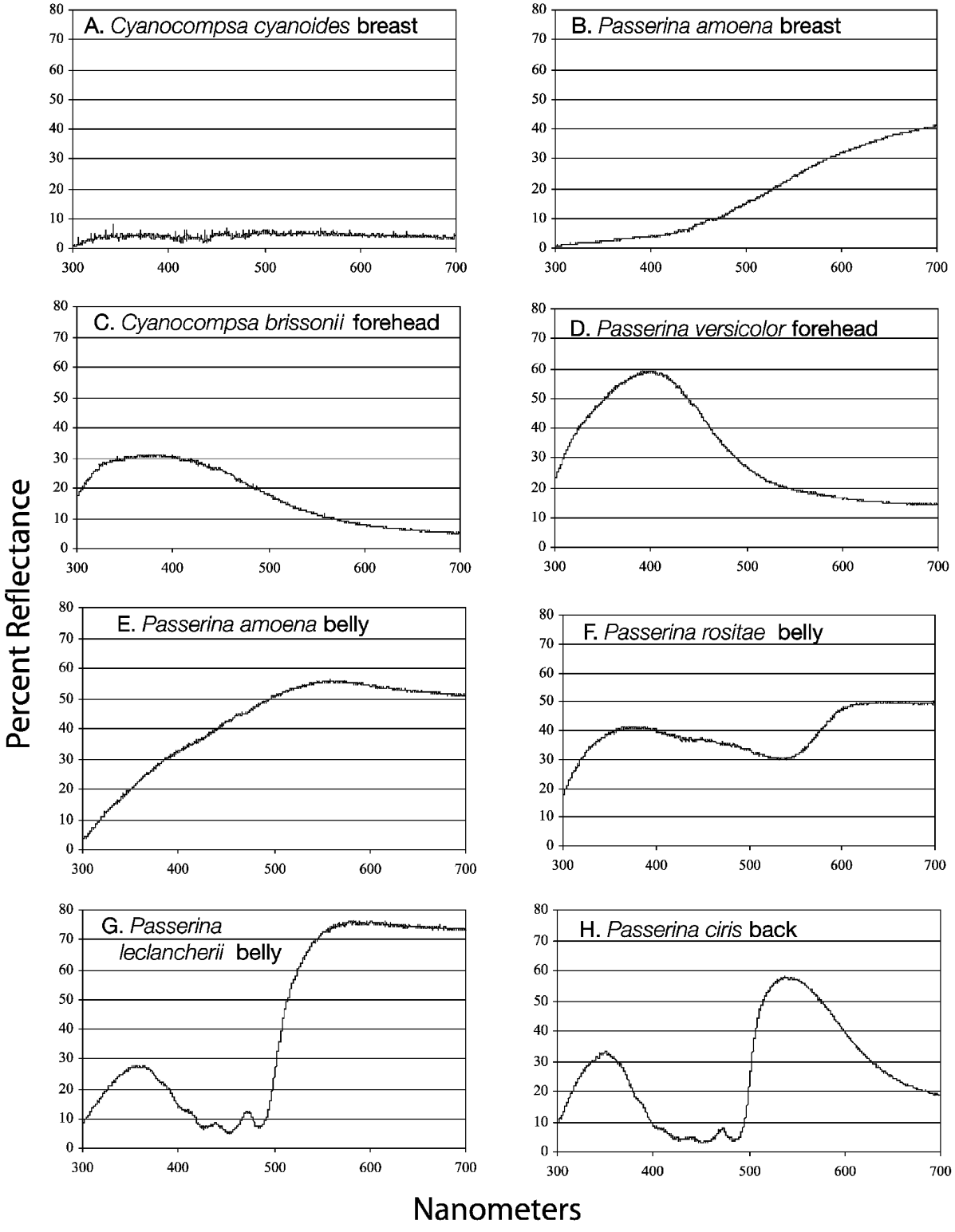

Figure 3: Sample of average reflectance spectra of plumage patches of individual specimens of male *Cyanocompsa* and *Passerina* buntings (Cardinalidae). *A*, Black breast of *Cyanocompsa cyanoides*; *B*, brown breast of *Passerina amoena*; *C*, ultraviolet blue forehead of *Cyanocompsa brissonii*; *D*, ultraviolet blue forehead of *Passerina versicolor*; *E*, "white" belly of *Passerina amoena*; *F*, pink belly of *Passerina rositae*; *G*, ultraviolet yellow belly of *Passerina leclancherii*; *H*, ultraviolet green back of *Passerina ciris*.

patterns and the availability of a robust phylogenetic hypothesis (Klicka et al. 2001). We measured color patches on 10 mature adult male representatives for each species using study skins from the Yale Peabody Museum of Natural History, New Haven, Connecticut, and the American Museum of Natural History, New York. Reflectance spectra were measured from six standard plumage patches: crown, back, rump, throat, breast, and belly. Reflectance spectra were measured three times per patch per individual. Additional color patches were also measured for certain species if they had additional colors that were distinct to the human eye, including forehead, epaulet, cheek, wing bar, lower belly, and nape. Most species had no additional color patches, although others had as many as three. The reflectance spectra of color patches were measured using an S2000 spectrometer (Ocean Optics, Dunedin, FL) with an Ocean Optics DH-2000-Bal deuterium-halogen light source. The average reflectance of each patch for each species was calculated by computing the specimen averages from the three replicate spectra measured for each individual for each data point between 300 and 700 nm and then averaging the 10 specimen spectra to obtain the species reflectance spectra for the patch. Analyses of individual variation are described below.

Tetrahedral Color Space

We developed a computer program—TETRACOLORSPACE—for the tetrahedral analysis of avian reflectance spectra, using MATLAB 7 software (MathWorks, Natick, MA). The program performs all of the tetrahedral analyses conducted in this article, and program MATLAB .m files are available from the authors or at http://www.yale.edu/eeb/prum/.

Following Goldsmith (1990), we estimated the idealized stimulus, Q_I, of each color cone type by the reflectance spectrum of a plumage patch:

$$Q_I = \int_{300}^{700} R(\lambda) C_r(\lambda) d\lambda, \quad (1)$$

where $R(\lambda)$ is the reflectance spectrum of the plumage patch, and $C_r(\lambda)$ is the spectral sensitivity function of each cone type r. The $R(\lambda)$ and $C_r(\lambda)$ functions were normalized to have integrals of 1. Following Goldsmith (1990), we treat irradiance $I(\lambda)$ as a constant across all visible wavelengths, with an integral equal to 1. We later examine the efficacy of this procedure with comparisons to Endler and Mielke's (2005) method incorporating ambient light spectra, von Kries color correction, and log transformation. The average spectral sensitivity curves of an ultraviolet cone–type retina from Endler and Mielke (2005, their supplementary online materials) were used.

The idealized stimulation values of the four color cones—Q_I— were normalized to sum to 1, yielding relative $\{u\ s\ m\ l\}$ values. Each plumage color pattern was described by a matrix of the $\{u\ s\ m\ l\}$ values for each patch in the plumage (table 1). The $\{u\ s\ m\ l\}$ values for each color patch were converted to a point with X, Y, and Z coordinates, following Endler and Mielke (2005). This tetrahedral geometry places the achromatic point of equal cone stimulation—white, black, or gray—at the origin and the UVS/VS, or u/v, vertex along the vertical Z-axis (fig. 1). The Cartesian (X, Y, Z) coordinates of each color point were then converted to its spherical coordinates θ, ϕ, and r, which define a color vector (fig. 1). For each species, the color vectors of all plumage patches were plotted as points in the tetrahedral color space, and overall color space occupancy was quantified.

Hue is defined as the direction of the color vector and is given by the angles θ and ϕ, which are analogous to longitude and latitude, respectively (fig. 1). Angle θ is the angular displacement of the color vector from the positive X-axis, which runs between the m (green) and l (red) vertices (fig. 1). Values of θ range from $-\pi$ to $+\pi$. Angle ϕ is the angular displacement of the color vector from the horizontal X-Y plane (fig. 1). Values of ϕ range from $-\pi/2$ to $+\pi/2$. The chroma, or saturation, of a color is given by the magnitude of r, or its distance from the achromatic origin. Colors of the same hue that differ in chroma are distributed on a single line at different lengths from the origin. Four functions that describe how variation in the relative stimulation of the four color channels—u, s, m, and l—varies as a function of chroma r for any given hue—θ and ϕ—are given in "Functions of Cone Stimulation for a Given Hue" in the appendix.

Because the color space is a tetrahedron and not a sphere, different hues vary in their potential maximum chroma, or r_{max}. The four pure hues at the vertices of the tetrahedron have $r_{max} = 0.75$. All other hues have $r_{max} < 0.75$, because a vector of any other hue with $r = 0.75$ would extend beyond the boundaries of the color space. The equations for r_{max} for any given hue are presented in "Maximum Chroma" (eq. [A11]) in the appendix. It may be more informative to define the chroma of a color relative to the maximum chroma possible for its hue rather than to its absolute difference from achromatic ($r = 0$) or the maximum chroma of a pure hue ($r = 0.75$). Consequently, we calculated the achieved chroma, $r_A = r/r_{max}$ for each color patch.

For each plumage, we computed the average color span, which is the average of the Euclidean distances between each pair of colors in the plumage (Δ_T of Endler and Mielke [2005]), and the variance in the color span. We

also estimated the volume of the color space occupied by the color patches of each plumage by calculating the volume of the minimum convex polygon that contains all the color points in the plumage. Additionally, we developed a new measure of contrast in hue that is independent of chroma. Hue disparity α is the magnitude of the angle between two color vectors (see "Maximum Chroma" in the appendix). We calculated the average hue disparity of all patches in each plumage, which gives a measure of overall hue contrast within a plumage. We also calculated the variance in hue disparity, which is a measure of the uniformity of hue contrast among plumage patches.

In our comparative analyses, we eliminated four patches of *Cyanocompsa brissonii* and five patches of *Cyanocompsa cyanoides* with <0.05 normalized brilliance (asterisks, table 1), because these patches were so dark that they yielded random hues.

Brilliance

For each color patch, we averaged the reflectance values for each 1-nm window between 300 and 700 nm. We measured peak percent reflectance (intensity), the wavelength λ_{max} of maximum reflectance, and normalized brilliance (total reflectance)/(100 × N), where total reflectance is the sum of percent reflectance at all data points between 300 and 700 nm and N is the number of data points between 300 and 700 nm ($N = 401$). In addition, we calculated the average percent UV reflectance (average u) of each plumage, which is a measure of the ultraviolet contribution to plumage color.

Comparing Color Spaces

We compared our application of Goldsmith's (1990) tetrahedral color space to Endler and Mielke's (2005) method for two representative species—*Cyanocompsa parellina* and *Passerina ciris*—under three different ambient light spectra. We repeated Endler and Mielke (2005) in calculating their Q_r, q_r, and the log-transformed q_r (for details, see "Detailed Methods," eqq. [A4], [A5], in the appendix). Irradiance spectra were collected with an Ocean Optics spectrophotometer, using a cosine corrector under typical forest cloudy, interior forest shade, and forest sunny-gap conditions (courtesy of M. Anciães). To understand the cumulative effects of each calculation on color space distributions, we generated normalized $\{u\ s\ m\ l\}$ and corresponding θ, ϕ , and r values based on Q_r, q_r, and log-transformed q_r values. We then compared these tetrachromatic color variables for individual patches and entire plumages for both species.

Comparative Phylogenetic Analyses

We examined the phylogenetic history of the evolution of color using the best-fit, maximum likelihood phylogeny of *Cyanocompsa* and *Passerina* by Klicka et al. (2001), which was based on sequencing of the mitochondrial cytochrome *b* gene in all species of the clade (Klicka et al. 2001). First, we examined patterns in the variation of continuous color characters, using the linear parsimony algorithm in MacClade 4.0 (Maddison and Maddison 2000). Then we used the computer program CONTINUOUS 1.0d13 (Pagel 1997, 1999) to investigate and compare alternative evolutionary models for the phylogenetic variation in color of the clade. We used the phylogeny and genetic distances from Klicka et al. (2001, their fig. 2*A*) to specify the tree topology and branch lengths in our analyses. In CONTINUOUS, we compared the log likelihoods of various alternative evolutionary models of the variation among 10 in-group species for eight plumage color variables: average color span, span variance, plumage color volume, hue disparity, the variance in hue disparity, average chromaticity, maximum chromaticity, and average brilliance (for details, see "Detailed Methods" in the appendix). We conducted analyses of intraspecific variation using two alternative methods, both of which confirmed the accuracy of using the species average spectra in comparative analyses (see "Analysis of Intraspecific Variation" in the appendix in the online edition of the *American Naturalist*).

Results

Plumage Color and Spectrophotometry

Reflectance spectra of the plumage patches of each species vary widely in shape and peak reflectance, representing a broad sample of the types of plumage reflectance spectra found within all birds (fig. 3; table 1). The wavelengths of peak reflectance of the bunting spectra range from 342 nm in various patches of *Cyanocompsa brissonii* and *Cyanocompsa cyanoides* to 700 nm in the red throat, breast, and belly of *Passerina ciris* (table 1). The diverse plumage colors in this clade are produced by a variety of presumed and known physical mechanisms, including eumelanin (fig. 3*A*), pheomelanin (fig. 3*B*), and carotenoid pigments (fig. 3*F*, 3*G*), structural colors produced by coherent scattering from spongy medullary keratin of feather barb rami (fig. 3*C*, 3*D*; Prum 2006), unpigmented white feathers (fig. 3*E*), and complex combinations of pigmentary and structural mechanisms (fig. 3*F*, 3*H*). All species contain at least one structurally colored plumage patch that appears merely blue to humans (fig. 2) but also reflects substantially in the ultraviolet range that is visible to birds.

The plumage colors of the *Cyanocompsa* species consist

almost entirely of blackish eumelanin-pigmented patches and structural ultraviolet/blue colors that appear to us as deep blue (fig. 2*A*). The plumage of *Passerina cyanea* is uniformly structural, with ultraviolet-rich blue and turquoise colors (fig. 2*B*). The plumage of *Passerina caerulea* and *Passerina amoena* are similar to that of *P. cyanea*, with additional deep red-brown patches produced by pheomelanin (fig. 2*C*, 2*D*) and an additional "white" belly patch (fig. 2*D*) in *P. amoena*, which is structural. In addition to blue colors, members of the "painted" bunting clade—*Passerina rositae*, *Passerina leclancherii*, *Passerina versicolor*, and *P. ciris*—exhibit a variety of carotenoid colors, including yellow, orange, and red (fig. 2*E*–2*H*). Other colors, such as the green back of *P. ciris*, purple in *P. versicolor*, and the pink belly of *P. rositae*, are apparently produced by a combination of carotenoid pigments and structural mechanisms. These reflectance spectra show two discrete peaks, one in the ultraviolet spectrum and another in the long visible spectrum (fig. 3*F*, 3*H*).

Species Plumage Patterns

Hue (θ, ϕ), chroma (r), achieved chroma (r_A), normalized brilliance, wavelength of peak reflectance (λ_{max}), and percent peak reflectance are given for all color patches in each species in table 1. Summary statistics calculated for the plumage of each species appear in table 2.

The tetrahedral plots of the colors of the plumage patches of each species show substantial variation and diversity in colors within and among plumages of male buntings. All three species of *Cyanocompsa* and *Passerina cyanea* are restricted to small regions of the ultraviolet/blue region of color space (fig. 4*A*–4*D*). All other species have some plumage patches in this ultraviolet/blue region of the color space but also have colors that extend into the highly chromatic red, yellow, and green regions of the color space (fig. 4*E*–4*J*).

Color span. Average plumage color span measures the overall color contrast among color patches in a plumage. Average color span values in the clade range over an order of magnitude, from 0.031 in *Cyanocompsa brissonii* to 0.30 in *P. ciris* (table 2). *Cyanocompsa* species and *P. cyanea* have low average color span values (<0.10) because the basically blue plumages are nearly monochromatic. The highly variable plumages of *P. ciris* and *P. leclancherii* (fig. 2*H*, 2*J*) yield a high average color span. *Passerina caerulea* also has a high average color span value (0.25) because of the high color contrast between its structural blue patches and the pheomelanin-based brown patches on its epaulet and wingbar.

Span variance is a measure of the uniformity of color contrast within a plumage. Span variance ranges over two orders of magnitude, from a minimum of 4.2×10^{-4} in *C. cyanoides* to a maximum of 5.5×10^{-2} in *P. caerulea*. *Cyanocompsa* have smaller span variances because their dark blue colors contrast with one another uniformly. *Passerina caerulea* has a much larger color span variance because the color pattern consists of only two highly contrasting colors, and the resulting bimodal distribution of spans has a high variance.

Plumage color volume. Plumage color volume is a measure of color diversity. Color volume ranges over four orders of magnitude within the clade, from 7.0×10^{-7} in *C. cyanoides* to 2.1×10^{-3} in *P. ciris* (table 2; fig. 4), and correlates well with a subjective impression of color diversity (fig. 2). Subjectively drab *C. cyanoides* and *C. brissonii* have the smallest color space volumes, while the diversely colorful species *P. ciris*, *P. rositae*, and *P. leclancherii* have the largest volumes. The range in color volume values is two orders of magnitude larger than the range in color span values because span is a linear measure and volume is a three-dimensional measure.

A plumage with a few highly contrasting colors in a linear or planar distribution may have a high color span but small color volume. The highly contrasting blue, brown, and white patches of *P. amoena* are linearly distributed, resulting in high span (0.17) but minimal volume (5.8×10^{-6}). Conversely, a pattern that consists of many different colors with small differences among colors may have a low span but large volume. For example, *P. versicolor* has an average color span of 0.14 but a substantially larger volume (2.1×10^{-4}).

Hue Disparity. The maximum hue disparity between patches within any male plumage in the clade occurs between the crown and the breast in *P. amoena* (2.2166), the crown and the back in *P. ciris* (2.2855), and between the breast and the nape or rump in *P. leclancherii* (2.428 and 2.5004, respectively). These highly disparate hues have hue complementarity values between 0.70 and 0.79 (see "Detailed Methods"). Mechanistically, these highest hue disparity values come from contrasts between a structural blue in each species and a pheomelanin brown in *P. amoena*, a carotenoid orange in *P. leclancherii*, and a probable combined structural and carotenoid green in *P. ciris*.

Average hue disparity of male bunting plumages ranges over two orders of magnitude, from a low of 0.08 in *C. brissonii* to 1.3 in *P. leclancherii* (table 2). In general, hue disparity correlates well with a subjective impression of hue variation, with low values in monochromatic species like *C. parellina*, *C. brissonii*, and *P. cyanea* and dramatically higher values in species with brown pheomelanin patches (*P. caerulea* and *P. amoena*) or carotenoid patches (painted clade species). Predictably, within the painted clade, hue disparity is notably lowest in *P. versicolor*, which has a plumage dominated by similar bluish, violet, and purple hues. Variance in hue disparity, an aspect of the uniformity

Table 1: Descriptions of the color and brilliance of all plumage patches measured from male *Cyanocompsa* and *Passerina* buntings (Cardinalidae)

Patch	% relative stimulation of color cones				Hue (radians)		Chroma (r)	r_{max}	Achieved chroma (r_A)	Normalized brilliance	λ_{max} (nm)	% reflectance at λ_{max}
	u	s	m	l	θ	ϕ						
C. brissonii:												
Crown	41.73	30.16	16.29	11.82	−2.85	.96	.20	.39	.53	.061	342	11.04
Back*	35.35	28.09	20.3	16.26	−2.96	.95	.13	.36	.35	.039	342	6.41
Rump	38.77	29.09	18.5	13.65	−2.93	.96	.17	.37	.45	.068	342	11.53
Throat*	30.01	23.28	23.09	23.62	−.87	1.50	.05	.66	.08	.035	342	5
Breast*	34.15	28.96	20.34	16.54	−2.92	.87	.12	.36	.34	.042	342	6.45
Belly*	31.1	25.11	22.6	21.19	−2.98	1.19	.07	.43	.15	.046	342	6.6
Forehead	41.14	32.75	16.02	10.09	−2.87	.84	.22	.36	.60	.178	378	31.03
Epaulet	39.11	31.24	17.51	12.14	−2.89	.86	.19	.36	.51	.249	342	41.78
Cheek	40.77	32.79	16.11	10.33	−2.87	.83	.21	.36	.59	.091	384	15.98
C. cyanoides:												
Crown*	24.11	21.58	28.98	25.33	1.04	−.19	.05	.34	.14	.020	342	4.21
Back*	22.67	22.05	29.34	25.93	1.01	−.48	.05	.43	.12	.025	342	4.57
Rump	25.73	24.37	26.61	23.29	1.90	.34	.02	.32	.07	.053	342	7.95
Throat*	13.2	17.41	32	37.39	.26	−.75	.17	.37	.47	.030	698	5.71
Breast*	22.56	24.67	28.09	24.68	1.57	−.79	.03	.35	.10	.041	342	6.02
Belly*	21.01	21.24	28.67	29.08	.48	−.64	.07	.42	.16	.042	558	5.93
Forehead	29.28	29.4	24.36	16.96	3.03	.51	.09	.27	.32	.081	342	12.1
Epaulet	29.26	27.86	24.21	18.68	3.02	.65	.07	.28	.25	.132	342	18.8
Cheek	25.86	28.12	26.31	19.71	2.82	.16	.05	.26	.21	.059	342	8.5
C. parellina:												
Crown	39.91	37.6	14.89	7.6	−2.85	.66	.24	.35	.70	.138	417	25.33
Back	41.12	34.52	14.57	9.79	−2.80	.79	.23	.37	.61	.060	389	11.23
Rump	39.11	36.88	15.61	8.4	−2.86	.66	.23	.35	.66	.197	430	34.78
Throat	35.19	35.01	16.95	12.84	−2.79	.61	.18	.36	.49	.074	437	12.23
Breast	38.12	33.73	16.03	12.12	−2.79	.75	.19	.37	.52	.080	389	13.7
Belly	37.03	35.93	16.17	10.87	−2.82	.64	.20	.36	.57	.068	430	12.22
Forehead	32.66	37.55	20.17	9.62	−3.0	.42	.19	.31	.62	.305	450	50.29
Epaulet	36.59	37.4	17.12	8.88	−2.90	.57	.21	.33	.64	.248	430	42.42
Cheek	37.23	39.53	16.07	7.17	−2.89	.54	.24	.33	.71	.167	430	30.77
P. cyanea:												
Crown	33.65	39.69	18.24	8.42	−2.93	.42	.21	.32	.66	.201	461	34.91
Back	25.53	28.23	31.98	14.26	2.42	.05	.11	.27	.43	.193	525	30.98
Rump	28.37	28.07	30.26	13.3	2.50	.29	.12	.25	.47	.237	524	35.88
Throat	30.48	39.81	21.54	8.18	−3.05	.27	.20	.30	.67	.196	479	35.07
Breast	28.42	37.27	24.46	9.85	3.10	.20	.17	.28	.61	.223	489	38.43
Belly	28	33.57	27.98	10.45	2.85	.20	.15	.26	.58	.240	503	40.52
P. caerulea:												
Crown	44	34.49	12.95	8.56	−2.78	.84	.25	.39	.66	.263	404	53.83
Back	34.39	32.57	18.26	14.78	−2.80	.68	.15	.36	.41	.101	422	16.08
Rump	38.64	35.31	15.42	10.62	−2.80	.71	.21	.37	.58	.209	409	38.6
Throat	45.72	33.56	12.25	8.47	−2.76	.90	.27	.40	.66	.199	400	41.59
Breast	44.97	33.7	12.58	8.75	−2.76	.88	.26	.40	.65	.186	396	38.74
Belly	42.37	34.33	13.6	9.7	−2.77	.82	.24	.39	.61	.20	404	40.49
Epaulet	5.2	10.46	29.54	54.79	−.08	−.63	.34	.43	.79	.080	698	25.18
Wingbar	7.58	16.05	31.79	44.57	.06	−.78	.25	.35	.70	.129	698	28.36

Table 1 (*Continued*)

Patch	% relative stimulation of color cones				Hue (radians)		Chroma		Achieved chroma	Normalized brilliance	λ_{max} (nm)	% reflectance at λ_{max}
	u	*s*	*m*	*l*	θ	ϕ	(*r*)	r_{max}	(r_A)			
P. amoena:												
Crown	24.96	32.24	30.61	12.2	2.69	0	.14	.27	.51	.362	511	61.01
Back	19.82	24.95	32.83	22.4	1.81	−.66	.08	.41	.21	.118	532	17.88
Rump	23.64	28.85	31.96	15.54	2.44	−.13	.11	.28	.38	.255	524	40.77
Throat	24.81	31.09	31.09	13.02	2.62	−.02	.13	.27	.48	.343	519	57.76
Breast	3.99	13.69	34.12	48.2	.11	−.78	.30	.36	.84	.178	698	41.1
Belly	13.29	25.06	31.19	30.46	.63	−1.23	.12	.26	.47	.419	558	55.85
Wingbar	13.9	24.97	31.24	29.89	.73	−1.22	.12	.27	.44	.323	558	43.26
P. rositae:												
Crown	40.7	40.6	12.2	6.51	−2.77	.61	.27	.37	.74	.3	438	57.41
Back	30.02	33.59	25.58	10.81	2.97	.34	.15	.26	.57	.218	501	34.46
Rump	32.04	34.74	23.46	9.75	3.09	.43	.17	.28	.61	.32	488	50.15
Throat	33.4	39.93	17.63	9.04	−2.89	.41	.21	.33	.64	.319	459	55.93
Breast	32.82	36.25	15.96	14.97	−2.66	.49	.17	.42	.40	.313	450	50.91
Belly	24.71	22.97	21.52	30.79	−.67	−.05	.06	.44	.14	.391	652	49.91
Low belly	19.07	15.95	25.73	39.25	−.09	−.39	.16	.43	.36	.37	637	59.88
Nape	35.87	39.46	17.73	6.93	−2.95	.49	.23	.32	.72	.226	459	38.91
P. leclancherii:												
Crown	14.13	3.31	50.84	31.72	.93	−.36	.31	.36	.87	.245	548	65.36
Back	25.81	20.84	36.93	16.42	1.78	.06	.13	.39	.34	.21	530	39.92
Rump	29.44	28.52	29.5	12.54	2.57	.36	.12	.25	.50	.304	516	48.02
Throat	9.32	3.6	38.29	48.79	.3	−.5	.33	.38	.86	.313	700	64.26
Breast	4.56	1.79	36.21	57.45	.14	−.54	.40	.43	.93	.285	652	68.43
Belly	12.54	6.16	39	42.3	.44	−.47	.27	.36	.75	.426	592	75.91
Nape	29.79	29.58	30	10.63	2.6	.34	.14	.25	.57	.278	512	47.5
P. versicolor:												
Crown	37.13	14.84	16.14	31.9	−.46	.81	.17	.41	.41	.113	378	18.58
Back	31.76	19.97	20.76	27.5	−.43	.93	.08	.42	.2	.072	378	10.28
Rump	42.41	32.93	13.95	10.71	−2.75	.87	.23	.4	.57	.237	404	45.55
Throat	39.21	17.61	16.97	26.21	−.59	1.15	.16	.48	.32	.09	384	16.17
Breast	47.71	17.38	14.59	20.32	−1.03	1.42	.23	.55	.42	.117	378	26.06
Belly	34.89	24.51	19.23	21.37	−2.2	1.25	.10	.45	.23	.086	394	13.86
Forehead	40.51	31.61	15.35	12.52	−2.76	.89	.20	.40	.50	.316	393	58.97
P. ciris:												
Crown	48.67	32.11	10.96	8.26	−2.72	.98	.29	.43	.67	.226	401	49.89
Back	19.45	6.46	45.29	28.8	.96	−.23	.25	.33	.74	.262	538	57.8
Rump	35.77	12.28	19.12	32.83	−.19	.70	.17	.33	.51	.176	351	27.62
Throat	20.19	10.44	18.06	51.32	−.35	−.18	.27	.46	.58	.21	700	45.85
Breast	17.84	7.35	15.46	59.35	−.38	−.21	.35	.50	.71	.193	700	49.73
Belly	19.67	9.12	18.6	52.61	−.31	−.19	.29	.45	.64	.219	700	49.52

Note: For *C. brissonii* and *C. cyanoides*, the plumage patches marked with an asterisk were not used in the calculation of summary color statistics because they have a normalized brilliance of <0.05.

of among-patch variation in hue, is highest in *P. caerulea*, *P. rositae*, and *P. leclancherii*—all species with multiple patches of different classes of pigmentary and structural colors.

A convenient graphical way to visualize hue disparity independently of chroma is to project the hue vectors of each color onto a unit sphere centered at the origin and to view the distribution of hues on the sphere, using the Robinson projection (Endler et al. 2005), which is commonly used to represent a map of the earth in two dimensions. The Robinson projections of the hues of a sample of six species demonstrate the extreme variation in patterns of hue disparity among species (fig. 5).

Chroma. Chroma *(r)* of individual plumage patches ranges from lows of 0.02 and 0.05 in the rump and cheek of *C. cyanoides* and 0.06 in the belly of *P. rositae* to max-

Table 2: Summary statistics describing plumage color and brilliance of male *Cyanocompsa* and *Passerina* buntings (Cardinalidae)

Species	Average color span	Variance of color span	Color space volume	Average hue disparity	Variance of hue disparity	Average achieved chroma (r_A)	Maximum achieved chroma (max r_A)	Average brilliance	Maximum brilliance
C. brissonii	3.1×10^{-2}	1.9×10^{-4}	5.3×10^{-7}	.08	2.2×10^{-3}	.54	.60	.09	.25
C. cyanoides	4.8×10^{-2}	4.2×10^{-4}	7.0×10^{-7}	.67	1.4×10^{-1}	.21	.32	.05	.13
C. parellina	4.6×10^{-2}	3.3×10^{-4}	2.0×10^{-5}	.15	9.1×10^{-3}	.61	.71	.15	.31
P. cyanea	9.2×10^{-2}	2.2×10^{-3}	2.5×10^{-5}	.50	6.8×10^{-2}	.57	.67	.21	.24
P. caerulea	2.5×10^{-1}	5.5×10^{-2}	1.9×10^{-4}	1.28	1.9	.63	.79	.17	.26
P. amoena	1.7×10^{-1}	1.3×10^{-2}	5.8×10^{-6}	1.12	4.8×10^{-1}	.48	.84	.29	.42
P. rositae	1.8×10^{-1}	1.4×10^{-2}	3.2×10^{-4}	1.28	1.3	.52	.74	.31	.39
P. leclancherii	2.8×10^{-1}	2.3×10^{-2}	3.2×10^{-4}	1.30	7.4×10^{-1}	.69	.93	.29	.43
P. versicolor	1.4×10^{-1}	3.4×10^{-3}	2.1×10^{-4}	.67	1.5×10^{-1}	.38	.57	.15	.32
P. ciris	3.0×10^{-1}	2.7×10^{-2}	2.1×10^{-3}	1.21	5.9×10^{-1}	.64	.74	.21	.26

imums of 0.35 in the breast of *P. ciris* and 0.40 for the breast of *P. leclancherii* (table 1). Achieved chroma values (r_A) range from 0.07 for the rump of *C. cyanoides* to 0.93 for the orange yellow breast of *P. leclancherii* (table 1). Average achieved chroma over the entire male plumage for each species ranges over threefold, from 0.21 in *C. cyanoides* to 0.69 in *P. leclancherii*. The maximum achieved chroma for all the plumage patches in each species ranges from a minimum of 0.32 in the ultraviolet forehead of *C. cyanoides* to a maximum of 0.93 in the orange breast of *P. leclancherii* (table 2), indicating that each species has at least one highly chromatic plumage patch.

There appears to be little consistent relationship within this clade between achieved chroma and color production mechanism. The patches with highest r_A are brilliant carotenoid patches (*P. leclancherii* breast and crown), combinations of carotenoid pigment and structure (*P. leclancherii* crown and *P. amoena* breast), and a pheomelanin-pigmented patch (*P. caerulea* epaulet). The patches with the lowest r_A are nonbrilliant structural patches (*C. cyanoides* rump and cheek, *P. amoena* back) and combined carotenoid-pigment and structural patches (back of *P. versicolor*, belly of *P. rositae*). Various color mechanisms are capable of achieving highly chromatic colors.

A regression of achieved chroma (r_A) versus chroma (r) for all plumage patches indicates a highly significant linear relationship ($b = 2.71$, $R^2 = 0.81$, $P = .000$). The sample of plumage patches with the highest and lowest achieved chromas includes patches from different species with a variety of plumage coloration mechanisms.

Interestingly, the apparently "white" belly of *P. amoena* (fig. 1) is not a genuine tetrachromatic avian white with equivalent reflectance across the entire visible spectrum (fig. 3*E*). Although the reflectance is uniformly high at longer wavelengths visible to humans (LWS [30.46%], MWS [31.19%], and SWS [25.06%]), the UVS stimulation has a notably lower value of 13.29% (table 1). Consequently, although this patch looks "white" to human vision, it is a very distinctive nonwhite color to tetrachromatic avian vision. The "white" belly of *P. amoena* is more chromatic—that is, has larger r—than several other plumage patches analyzed, including *P. amoena*'s own blue rump ($r = 0.12$ vs. 0.11, respectively; fig. 2; table 1). *Passerina amoena*'s white belly also has higher achieved chroma ($r_A = 0.47$) than many other plumage patches analyzed, including *P. amoena's* blue back ($r_A = 0.21$; table 1).

Brilliance. Average brilliance ranges over an order of magnitude, from 0.05 in *C. cyanoides* to 0.31 in *P. rositae* (table 2). Maximum patch brilliance for each species ranges more than threefold, from a minimum of 0.13 in the blue epaulet of *C. cyanoides* to a maximum of 0.43 in the yellow belly of *P. leclancherii* (tables 1, 2). The peak wavelength of the patch with the highest percent reflectance in each species ranges from 342 nm in the ultraviolet epaulets of *C. brissonii* and *C. cyanoides* to 637 nm in the pink lower belly of *P. rositae* (table 2).

Ultraviolet color. Values of u provide a tetrachromatic estimate of the ultraviolet stimulation component of each color patch (table 1). In general, structurally colored patches have higher (>achromatic null of 25%) values of u, whereas pheomelanin and certain carotenoid patches have the lowest u values. Average u values of whole plumages range from a low of 17.77% in *P. amoena* to a maximum of 40.31% in *C. brissonii*. Maximum u of individual color patches ranges from a minimum of 24.96% in the blue crown of *P. amoena* to a maximum of 48.67% in the blue crown of *P. ciris*.

In contrast, values of ϕ provide the ultraviolet component of hue (table 1). All structurally colored patches of *Cyanocompsa*, *P. cyanea*, and *P. caerulea* have positive ϕ values, indicating hues in the upper, ultraviolet region of the color space or above the equator in the Robinson projections of hue (fig. 5). Species of the painted clade

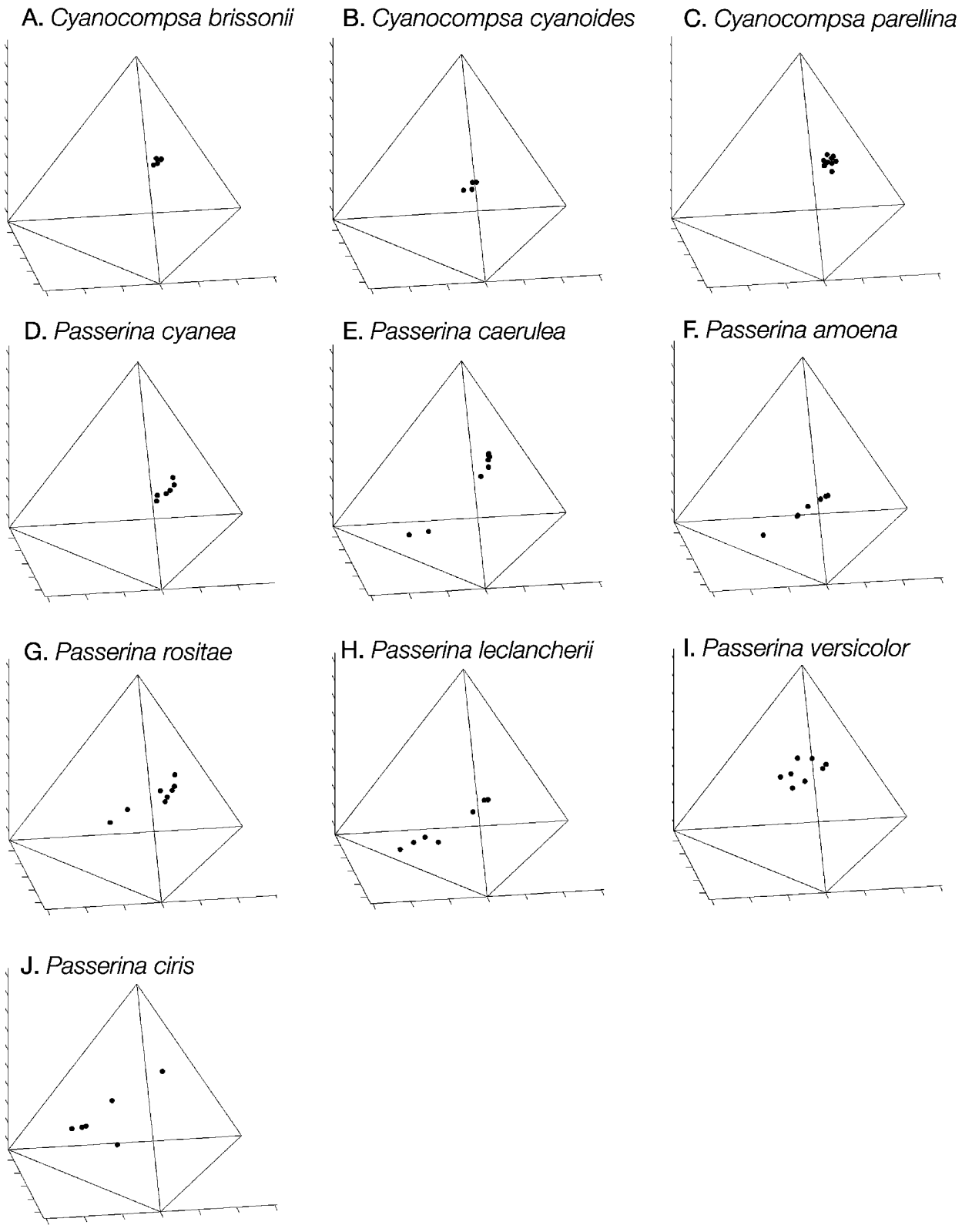

Figure 4: Distributions of the colors of the plumage patches of male *Cyanocompsa* and *Passerina* buntings in the tetrahedral color space.

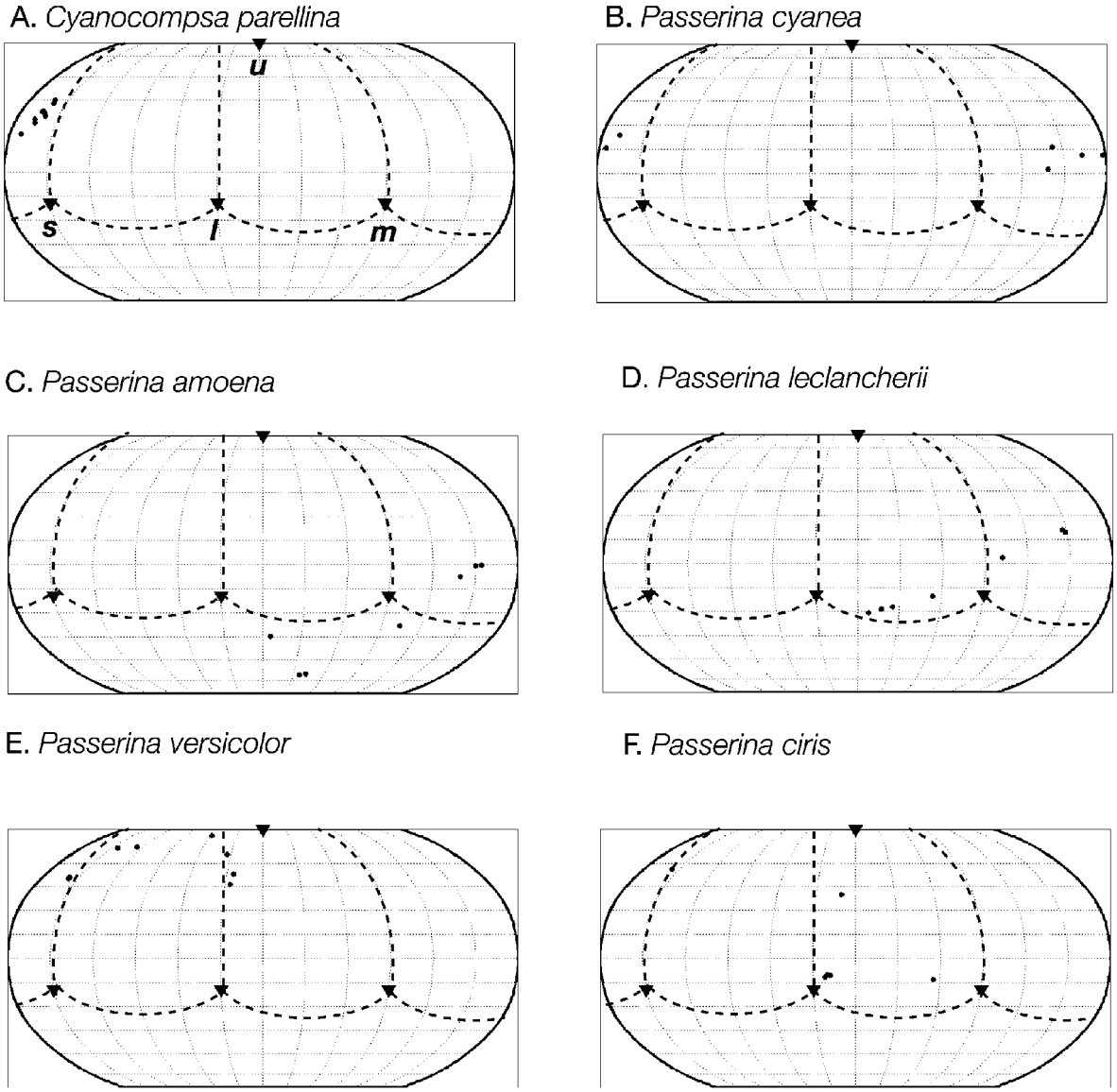

Figure 5: Robinson projections of the hues of the plumage patches of males of six species of *Cyanocompsa* and *Passerina* buntings. *A*, *Cyanocompsa parellina*; *B*, *Passerina cyanea*; *C*, *Passerina amoena*; *D*, *Passerina leclancherii*; *E*, *Passerina versicolor*; *F*, *Passerina ciris*. The distribution of dots indicates the variation in hue among the colors of the plumage patches of each species, given by the azimuth and elevation angles θ and ϕ, equivalent to longitude and latitude, respectively. The hue vectors are projected onto a sphere centered at the achromatic origin, and the sphere is depicted using the Robinson projection, a two-dimensional representation of the surface of the earth. Triangles indicate the *u*, *s*, *m*, and *l* vertices of the tetrahedron (labeled in *A*). The dotted lines indicate the spherical projection of the four edges of the color tetrahedron. The data are projected as if the observer were looking downward onto the equator of the spherical surface.

have patches with both positive and negative ϕ values. *Passerina amoena* is unique in having entirely negative ϕ values; all *P. amoena* hues are in the lower quadrant of the color space, or the southern hemisphere of the Robinson projection (fig. 5*C*).

Comparing Color Spaces

We compared the idealized stimulus color space of Goldsmith (1990) to a more detailed model of color perception of Endler and Mielke (2005), using plumage reflectance

of two representative bunting species and representative ambient irradiance spectra from forest shade, forest cloudy, and forest sunny-gap environments. When we calculated Q_r, which incorporates the ambient light spectrum (eq. [A4]), and projected these $\{u\ s\ m\ l\}$ values into the color space, we obtained major changes in hue and chroma that reflected the differential availability of ambient light in the irradiance spectrum. However, when we subsequently calculated q_r by applying the von Kries transformation for color constancy (eq. [A5]) by dividing Q_r by the integral of the product of the irradiance and cone sensitivity spectra, the resulting $\{u\ s\ m\ l\}$ values converged to within a few tenths of a percent of the $\{u\ s\ m\ l\}$ values from the Goldsmith (1990) idealized color space (Q_i; eq. [1]). Consequently, the tetrachromatic hues and chromas of the q_r values were extremely similar to the values obtained for the idealized signal space, Q_i. The θ and ϕ values varied by as much as a few tenths, and r values varied by as much as a few hundredths. The results were the same for all three ambient light conditions. Incorporating both ambient light variation and color constancy corrections (q_r; eq. [A5]) produces results that were essentially identical to results when assuming an idealized, constant illumination (Q_i; eq. [1])

When we log transformed the q_r values, as recommended by Endler and Mielke (2005), the resulting $\{u\ s\ m\ l\}$ values created substantial changes in hue and even larger decreases in chroma (r). For example, in *P. ciris*, chroma values declined by an order of magnitude, and hue disparity declined similarly. By greatly homogenizing variation among the quantal catches of the cone types, the log transformation of the $\{u\ s\ m\ l\}$ cone stimuli has complex effects on hue and produces large reductions in chroma and color contrast.

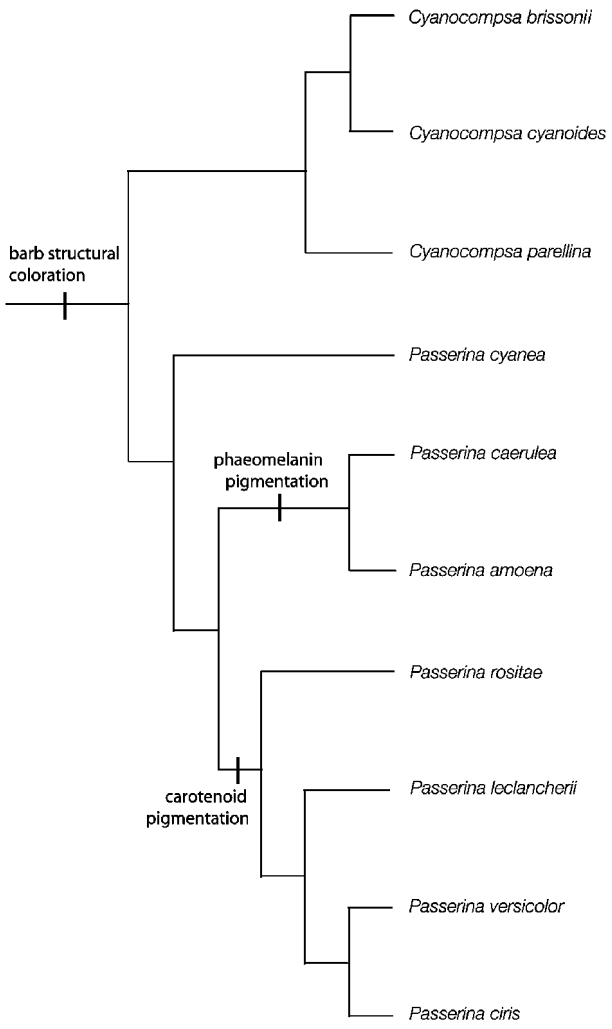

Figure 6: Phylogeny of *Cyanocompsa* and *Passerina* buntings by Klicka et al. (2001). Relative branch lengths are not depicted. Three major evolutionary novelties in male plumage coloration mechanism are shown: the origin of structural coloration produced by spongy medullary barb keratin, the origin of pheomelanin pigmentation, and the origin of carotenoid pigmentation. Each plumage color mechanism innovation is associated with major evolutionary shifts in the occupancy of the color space.

Evolution of Plumage Color

The basal species within the bunting clade—*Cyanocompsa* and *P. cyanea*—have male plumages restricted to the ultraviolet/blue regions of the color space (figs. 4, 6). Male plumages of two subclades have independently expanded into the saturated red-yellow-green regions of the color space with the evolution of pheomelanin expression in the *P. caerulea–P. amoena* clade and carotenoid expression in the painted bunting clade (figs. 4, 6).

Color span. The ancestral plumage had a low average color span and low color contrast. Average color span increased in lineages leading to both the *P. caerulea–P. amoena* clade and the painted clade, with *P. caerulea*, *P. leclancherii*, and *P. ciris* evolving the highest average color spans. Color span and the variance of color span are highly correlated (data not shown).

Plumage color volume. The ancestral plumage occupied a small color volume and probably increased twice independently, once in *P. caerulea* and once in the painted clade (fig. 7*A*). Alternatively, it is possible that there was a single increase in plumage volume, with subsequent loss of volume in *P. amoena* (fig. 7*A*). However, differences in the molecular pigments that have evolved in these lineages support the conclusion that these increases in color volume have been phylogenetically independent. The maximum color volume was subsequently achieved in *P. ciris* (fig. 7*A*).

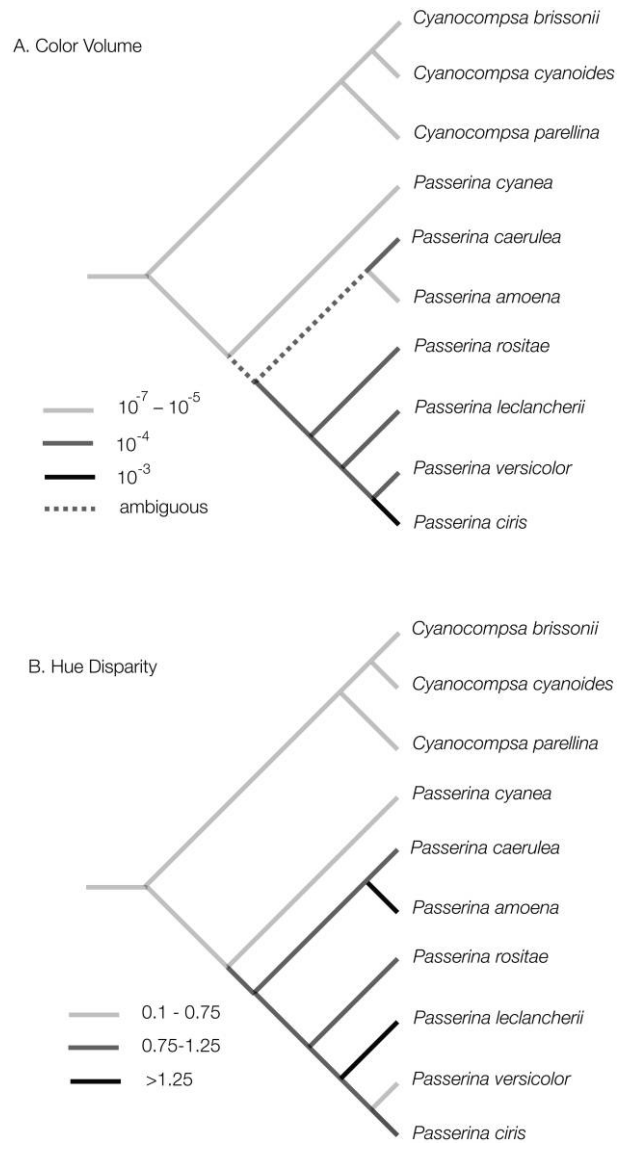

Figure 7: Linear parsimony optimizations of the evolution of two continuous color space variables for species of *Cyanocompsa* and *Passerina* buntings on the phylogeny of Klicka et al. (2001). *A*, Color volume; *B*, average hue disparity.

Hue Disparity. The ancestral plumage was dominated by structural blue/ultraviolet patches (fig. 4) with low average hue disparity (<0.75; fig. 7*B*; table 2). Hue disparity increased in the clade including all *Passerina* except *cyanea*, with subsequent further increases in *P. amoena* and *P. leclancherii* to the maximum values in the clade and a reversal in *P. versicolor* to the low ancestral values (fig. 7*B*). Variance in hue disparity was highly correlated with disparity, showing extreme derived values in *P. amoena* and *P. leclancherii*.

Chroma. Changes in average achieved chroma appear to have been unconstrained, occurring independently in several lineages without clear trends (table 2). Average achieved chroma of the whole plumage appears to have decreased in *C. cyanoides* and increased independently in *P. caerulea*, *P. leclancherii*, and *P. ciris*. Alternatively, average achieved chroma could have increased in the common ancestor of *P. leclancherii*, *P. versicolor*, and *P. ciris* and then been secondarily reduced in *P. versicolor*. Similarly, maximum achieved chroma evolved independently in different lineages with little evident trend (except positive association with carotenoid expression). Maximum achieved chroma varies widely among even the most closely related species of *Passerina*.

Brilliance. The ancestral plumage was only moderately brilliant. Average brilliance decreased in *C. cyanoides* and increased in various *Passerina*. It appears that highly brilliant patterns in *Passerina* were also secondarily lost in *P. amoena* and *P. versicolor*. The most brilliant plumage patches of the most basal lineages within the clade—*Cyanocompsa* and *P. cyanea*—are all structural blues and ultraviolet colors, implying that the ancestral condition was likewise. The patches with the highest peak percent reflectance in the clade are produced with carotenoid-pigmented yellow (*P. leclancherii* belly at 76% peak reflectance) and pink (*P. rositae* belly at 60%). However, within the same painted clade, *P. versicolor* has secondarily evolved a plumage with entirely low-wavelength peaks (between 375 and 400 nm) and substantially lower average brilliance.

Models of Plumage Color Evolution

We first compared an undirected random walk evolutionary model (CONTINUOUS model A; equivalent to the Brownian motion model of Felsenstein [1985]) to a directed-change evolutionary model that allows each color variable to evolve in a directed manner (either positive or negative) with evolutionary distance since common ancestry (CONTINUOUS model B; equivalent to the directional selection model of Martins and Hansen [1997]). The directed evolution model yielded a much better fit to the phylogenetic data than the random walk model (ln likelihood ratio = 12.3317, $P = .00177$). The GLS estimates of β values—the slopes of evolutionary change with distance—were positive for each color variable except for average achieved chroma and average brilliance (data not shown).

We then examined directed evolutionary models with variation in additional evolutionary parameters: κ, a scaling factor that weights longer or shorter branches in evolutionary history; δ, a scaling factor that changes the rate of evolution across all lineages over time; and λ, the overall weight of the contribution of phylogenetic correlation to

the variation in the data. In a series of log-likelihood tests, we compared a null directed-evolution model using the default parameter values (κ, δ, $\lambda = 1$) with alternative models using the maximum likelihood estimate (MLE) values of κ, δ, and λ.

The MLE value of κ was 3, the maximum allowed. This evolutionary model increases the impact of longer phylogenetic branches on color character evolution compared to the null model. The log likelihood of MLE κ model was significantly higher than that of the null directed-change model with uniform weight to branches of different lengths (ln likelihood ratio = 23.77, $P = .0000$).

The MLE value of δ was 3, the maximum allowed. This model accelerates color evolution over evolutionary time in comparison to the null model. The MLE δ model had a significantly higher log likelihood than that of the null directed-change model with uniform evolutionary rates (ln likelihood ratio = 19.675; $P = .000$).

The MLE value of λ was 0, the minimum value that completely eliminates all phylogenetic correlation among the species values for all variables. The nonphylogenetic ($\lambda = 0$) model also provided a significantly better fit to the data than the null directed-change evolution model (ln likelihood ratio = 6.99262, df = 1, $P = .000184251$). Accordingly, an evolutionary model that entirely ignores the phylogenetic relationships provides a better explanation of the color data than the fully phylogenetic null model ($\lambda = 1$). (The same result holds for a similar comparison using the undirected random walk model [model A; MLE value of $\lambda = 0$; ln likelihood ratio = 21.7309, $P = .0000$].)

The overall best-fit model identified used the MLE values of $\kappa = 3$, $\delta = 3$, and $\lambda = 0$. The model had the highest overall ln likelihood (203.169). In summary, in the best-fit, nonphylogenetic, directed-change model, bunting species have independently evolved to be more colorful—more extreme in multiple measures of color—since their most recent speciation event. In six of eight variables, values increased in magnitude since common ancestry (i.e., the slopes of the regressions of color variables with evolutionary distance; $\beta > 0$). However, bunting lineages have evolved plumage with significantly lower average brilliance since common ancestry; the ancestral average brilliance was estimated as $\alpha = 0.21$ and $\beta < 0$. As expected, correlation coefficients among color variables calculated from the highest likelihood directed-change model were overwhelmingly and substantially positive, except for average achieved chroma and average brilliance (data not shown).

Phylogenetic analyses of the continuous color trait variables indicate that color evolution in this bunting clade has been dominated by dynamic and accelerating rates of change in the most recent branches of the phylogeny (i.e., in each individual species). These recent changes have extensively erased the role of shared phylogenetic history in predicting the variation in color variables among species.

Discussion

Recent advances in our understanding of avian color vision and the phylogenetic relationships of birds now make it possible to examine how plumage coloration has evolved in an avian-appropriate color space. We have applied Goldsmith's (1990) tetrachromatic avian color space in our analysis of the evolution of plumage reflectance in a clade of New World buntings. These results provide a comparative natural history of plumage color evolution in the *Cyanocompsa-Passerina* clade and a detailed phylogenetic analysis of the evolution of multiple measures of plumage color in a diverse radiation. In addition, we have developed new measures of achieved chroma, hue diversity, and color space occupancy to complement those of Endler and Mielke (2005). Together, these graphical and computation tools for the tetrachromatic analysis of avian color variation create new opportunities for comparative analysis of evolutionary changes in coloration and color space occupancy.

Color Evolution in the New World Buntings

Both linear parsimony and generalized least squares (GLS) regression models of the evolution of plumage color measures in this New World bunting clade support the conclusion of an explosive evolutionary radiation in color space, especially in *Passerina*. Both methods detected positive trends in the evolution of most plumage color variables among these bunting plumages, but the overall pattern is of a rampant radiation. In the linear parsimony analyses, most individual color variables showed complex patterns of variation that cannot be described by simple phylogenetic trends. Indeed, the best-fit quantitative model of color evolution in the clade was a nonphylogenetic, directed random walk model with accelerating rates of evolution (CONTINUOUS model B, $\kappa = 3$, $\delta = 3$, $\lambda = 0$). Thus, variation in plumage color variables among species is predominantly explained by recent evolutionary changes unique to individual species lineages. Color evolution in the clade has been so dynamic that the signal of phylogenetic history in the evolution of color variables has been erased (Prum 1997).

This New World bunting clade was chosen for this study because of the diversity in plumage coloration and the availability of a corroborated phylogeny, but this clade is so diverse in plumage color that no single phylogenetic model can efficiently explain the evolution of color across the entire phylogeny. We do not predict that this quantitative result is generalizable across avian plumage col-

oration; rather, it reflects the specific phylogenetic history of color evolution in this clade.

In CONTINUOUS, the quantitative regression models apply over the entire phylogeny and do not permit the analysis of distinct models of evolution to different lineages within the clade. Although our quantitative analyses reject the role of phylogeny in any general model of plumage color evolution across the whole clade, there are strongly phylogenetic components to coloration within subclades. When evolutionary processes are heterogeneous, there is a possibility of a phylogenetic component to that heterogeneity.

There are some obvious qualitative changes in color across the *Cyanocompsa-Passerina* clade that demonstrate an important role for phylogeny in understanding the history of color evolution in the clade. The three species of *Cyanocompsa* are strikingly similar in plumage color, and this is reflected in their similar color space variables (fig. 1; tables 1, 2). Their shared plumage color patterns doubtless are homologous traits inherited from the common ancestor of the group. These phenotypic similarities in color were used by traditional systematists to classify them as congeners long before the monophyly of *Cyanocompsa* was confirmed by molecular phylogenetics (Klicka et al. 2001).

Given the ubiquity of structural blue colors in the *Cyanocompsa-Passerina* clade and their near absence in other cardinalids (except for *Cyanoloxia glaucocaerulea*, which may be the sister group to this clade), a broader phylogenetic analysis would probably identify a strong phylogenetic component to the structural blue plumage colors within the clade (see "Note Added in Proof"). The ancestral lineage of this New World bunting clade evolved a novel mechanism of structural plumage coloration and thereby pioneered new regions of the cardinalid color space (fig. 6). Thus, rejection of a significant component of phylogenetic variation in a single quantitative model of plumage color evolution in a clade does not falsify the role of phylogeny in explaining the origin and diversification of patterns in color evolution within the clade.

Two derived novelties in male plumage coloration mechanism are evolutionary innovations (and synapomorphies) of specific lineages within *Passerina*, and both contribute directly to evolutionary change in plumage color space occupancy (fig. 6). The male plumage of the *Paserina caerulea–Passerina amoena* clade is characterized by the derived expression of brown pheomelanin pigments in various male plumage patches. The evolution of pheomelanin expression in male plumage is associated with a derived increase in plumage color span within the ancestor of the *P. caerulea–P. amoena* clade. Likewise, the expression of carotenoid pigments in the male plumage of the ancestor of the painted clade is a coloration mechanism innovation of this clade. Carotenoid expression contributes to the wide variety of derived plumage colors, including purple, UV-red, red, pink, yellow, UV-yellow, and UV-green in the painted clade (figs. 1, 2). This phylogenetic novelty contributes to the tremendous color span, volume, and hue disparity within this subclade (e.g., fig. 7). Therefore, the evolution of male carotenoid pigmentation contributes directly to the rejection of a singular quantitative phylogenetic model of color evolution in the clade, even though the evolution of male carotenoid expression is itself a derived phylogenetic innovation that occurred within a specific clade.

Although we did not explore female plumage color in the clade, it is important to note that uniform pheomelanin brown female plumage is plesiomorphic with slight variation between redder browns and dusty browns. Greenish combined structural/carotenoid plumage colors have evolved in female plumages of *Passerina leclancherii* and *Passerina ciris* either convergently or with a secondary reversal to brown in female *Passerina versicolor*.

Innovation in Color Space

Endler et al. (2005) defined evolutionary elaborations in color as a linear translation of the distribution of color points in color space along the primary axis of color variation (i.e., principal component 1) and evolutionary innovations in color as orthogonal expansions of the distribution of color points in color space (i.e., principal component 2). In contrast, we define evolutionary innovations as qualitative rather than quantitative changes in the physical and biological mechanisms of color production themselves (Müller and Wagner 1991). Because Endler et al. (2005) used principal components analysis (PCA) to identify the primary linear axis of a distribution of color points, their definitions can lead to identifying some novel colors that are achieved through qualitative, mechanistic innovations as simple evolutionary elaborations. For example, *P. caerulea* and *P. amoena* (fig. 2*E*, 2*F*) have strikingly linear distributions of plumage colors (fig. 4) composed of plumage patches that are produced by coherent scattering, incoherent scattering, and pheomelanins. If the common ancestor of *P. caerulea* and *P. amoena* had structural blue and pheomelanin patches, then the mechanistic innovation of incoherently scattered white plumage in *P. amoena* would be an innovation by our definition. However, this white would not be considered a color innovation by Endler et al. (2005), because the color vectors of the white patches lie close to the line between the plesiomorphic structural blue and pheomelanin patches (fig. 2).

Comparing Color Spaces

Color spaces represent quantitatively the relationships among the spectral attributes of objects in a heuristic and pragmatic way. Unlike direct measurements of reflectance spectra themselves, color spaces rely on psychophysical models to describe the connection between stimuli and sensory experience (Kuehni 2003). Measurement theory, which provides the theoretical framework for the quantitative mapping of scientific observations, postulates that measurements are not the same as the things being measured (Kuehni 2003; Hand 2004). Thus, there exist multiple possible heuristic maps to depict the same quantitative observations. Since quantitative representations of sensory experience are not equivalent to the sensory experiences themselves, they cannot be more than convenient labels of perceptual experiences (Kuehni 2003). Quantitative mapping of measurements also includes both representational and pragmatic components (Hand 2004). Selecting an appropriate color space for comparative analysis requires a trade-off between the representational and pragmatic benefits, computational complexity, and generality.

The history of human color science documents that no single color space can represent the complexities of trichromatic human color perceptions in a uniform manner over multiple contexts but that many different color spaces provide consistent, quantitative insights into color perception and categorization, under limited circumstances (Kuehni 2003). Alternative human color spaces make different decisions about the scale of mapping, the standardization of observers, illuminations, and backgrounds. Also, each color space must focus on quantifying a specific level in the complex cascade of physical and psychological processes involved in color perception, from the stimulus reflectance to ambient environment and context, to cone absorption, to nerve excitation, to peripheral neural processing, to central processing, and to whole sensory experience (Kuehni 2003). Each successive level of psychophysical process included in the color space mapping brings additional assumptions and complexity and less generality.

Here, we have applied a tetrahedral color space from Goldsmith (1990) that incorporates reflectance spectra and the cone sensitivity spectra only. Recently, Endler and Mielke (2005) have applied a more detailed model of sensory perception that additionally incorporates ambient light spectra, color constancy, and log transformation of the cone color channels. Endler et al. (2005) propose their more complicated color space as a model of receiver sensory experience, or colors "as birds see them" (Endler and Mielke 2005). For many who are interested in studying color perception, function, and evolution in birds and other tetrachromatic vertebrates, the critical question will be which color space to use.

Human color science demonstrates that color sensations are produced by complicated poststimulus opponent processing among the trichromatic cone channels (Hurvich 1981; Kuehni 2003). For more than a century, followers of Helmholtz and Hering have produced alternative literatures proposing stimulus color spaces and opponent/sensory color spaces, respectively, to describe human color perception (for historical discussion, see Kuehni 2003). The color spaces of both Goldsmith (1990) and Endler and Mielke (2005) are stimulus spaces (following Helmholtz), and neither incorporates poststimulus opponent processing that is necessary to describe sensory perception fully. Goldsmith and Butler (2005) provide new empirical evidence of at least three opponent channels in budgerigars (*Melopsittacus undulatus*)—UV/S, S/M, and M/L, where S, M, and L represent short, medium, and long wavelength cone types, respectively. A new avian color space could be designed on the basis of their data. However, tetrachromacy creates a geometrical increase over trichromacy in the number of possible opponent processes, and Goldsmith and Butler's (2005) documentation of three opponent channels does not rule out the possibility that additional avian opponent channels exist. Without incorporating opponent processes and many other additional psychological features, Endler and Mielke's (2005) color space falls short of modeling plumages "as birds see them."

Does Endler and Mielke's (2005) color space provide additional empirical advantages over the simpler and more applicable Goldsmith (1990) color space? Our analysis indicates that it does not. Incorporating the effect of ambient light on estimates of quantal capture (Q_r; eq. [A4] in the appendix) does, by itself, have a large influence on quantitative descriptions of hue and chroma. However, transformation of stimulus estimates to account for color constancy correction (q_r; eq. [A5] in the appendix) eliminates this effect entirely. This von Kries transformation normalizes each cone stimulus magnitude by the stimulus of a flat (achromatic) reflectance under that ambient light. For the avian visual system under natural ambient light spectra, our calculations show that the von Kries transformation is highly effective. The Goldsmith (Q_i) and Endler and Mielke (q_r) estimates of cone stimuli yield essentially identical color space vectors under natural illumination.

Why does the von Kries transformation work so well? The mathematical conditions under which the von Kries transformation produces color constancy have been well established (West and Brill 1982). Further, many aspects of vertebrate color vision physiology have evolved to enhance color constancy, and some of these features are highly derived and extremely efficient in birds, for ex-

ample, minimizing overlap in cone sensitivity functions through the use of high-pass carotenoid filters in the cone oil droplets (Vorobyev et al. 1998, 2001; Hart 2001; Vorobyev 2003). It would be possible to subvert color constancy (i.e., create avian chromatic optical illusions) with artificial ambient light spectra, but for natural ambient light spectra, the von Kries transformation effectively eliminates distortions in hue and chroma that result from differential availability of wavelengths across the visual spectrum.

In contrast to the predictions of the sensory drive model (Endler and Basolo 1998), Endler et al. (2005, p. 1800) recently concluded that variation in ambient light has "small effects" in comparison to the overall patterns of variation in color space occupancy of the plumages, bowers, and backgrounds of bowerbird species. Even though their method uses ambient light variation in the estimation of receiver phenotype, Endler et al. (2005) used an unspecified "mixture" of woodland shade and open/cloudy ambient light spectra in their color space calculations. Thus, Endler et al. (2005) essentially controlled for ambient light variation within and among species by using a single standardized light environment. The Goldsmith color space achieves the same result in a more pragmatic way. If one accepts the voluminous evidence that multiple aspects of the avian visual and nervous system have evolved for advanced color discrimination and color constancy (Vorobyev et al. 1998, 2001; Vorobyev 2003), then Endler and Mielke's (2005) color space provides identical results to, and no additional advantage over, the simpler Goldsmith (1990) space. However, Endler and Mielke's (2005) color space requires substantially more environmental data, which are not commonly available. Minimally, our analysis indicates that environmental ambient light spectra are not necessary to conduct comparative color space analyses.

The capacity for visual color constancy correction has broad and important implications for avian plumage signal evolution. Environmental variation in the composition of ambient light has been well documented (e.g., Endler 1993). A diversity of avian plumage color signals are now hypothesized to have evolved through sensory drive by natural selection on signal receiver preferences for efficiency of color discrimination under different ambient light spectra (e.g., Endler and Théry 1996; Endler and Basolo 1998; Heindl and Winkler 2003). Given that color constancy is a fundamental feature of avian, and indeed basal vertebrate, color vision (Vorobyev et al. 1998, 2001; Hart 2001; Vorobyev 2003), opportunities for variation in ambient light spectral composition to affect avian color discrimination and visual efficiency should be quite limited. Despite recent correlative literature on sensory drive evolution in avian visual signals, it remains to be demonstrated that variation in ambient light spectral composition among environments creates any challenges or constraints to sensory efficiency of the tetrachromatic color visual systems of birds. Evolution in plumage coloration in response to variation in ambient light spectral composition through sensory drive has not been demonstrated, and the result of Endler et al. (2005) and our comparative analyses imply that it may not be expected to occur at all. Because the avian visual system is much better than ours at color discrimination and color constancy (e.g., Vorobyev et al. 2001), our own color experience should be a great exaggeration of the potential for avian color confusion.

Finally, the method of Endler and Mielke (2005) and Endler et al. (2005) includes the log transformation of the quantal catch estimates before normalizing to produce the $\{u\ s\ m\ l\}$ values for color space projection. In our repetition of this log transformation on bunting plumages, we obtained substantial changes in hue and dramatic reductions in chroma and span in comparison with the untransformed values. Although the effects of log transformation will depend on the scale of the quantal catch estimates, it will generally function to homogenize variation among the cone stimuli, decrease chroma, and decrease color differentiation. When input functions are normalized to integrals of 1, the quantal catch values are of small magnitude and log transformation produces dramatic changes.

Clearly, log transformation of quantal catch values before projection into color space can have profound, complex, and poorly understood effects on estimates of hue, chroma, and color space occupancy. This log transformation has been justified as an application of Fechner's law, which states that sensation is proportional to the logarithm of the stimulus intensity (e.g., the decibel scale of volume; Kuehni 2003; Vorobyev 2003). However, many examples of violations of Fechner's law have been found in human color vision, and alternative scaling functions have been proposed (Kuehni 2003).

Based on its unpredictable effects, we do not think that the log transformation of the quantal catch estimates is advisable or even justified. Endler and Mielke (2005) cite Vorobyev et al. (1998) for this procedure, but Vorobyev et al. (1998) did not apply it in calculating just-noticeable differences between a stimulus and a similar background; nor did they log transform the data in their tetrahedral projections of bird plumage spectra using Goldsmith's (1990) color space (Vorobyev et al. 1998, their fig. 4). Given that so many anatomical, physiological, and molecular details of the avian visual system have evolved to enhance color differentiation, the perception of chroma, and color constancy (Goldsmith 1990; Vorobyev et al. 1998; Hart 2001; Cuthill 2006), it seems unlikely that the

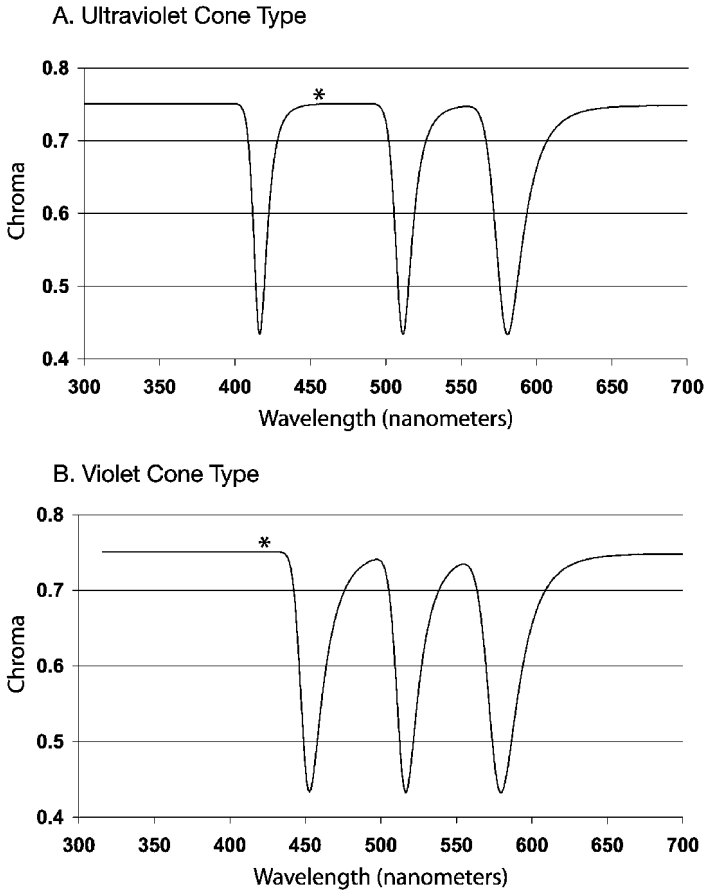

Figure 8: Variation in the chroma of monochromatic illumination across the avian visible spectrum from 300 to 700 nm for an avian UV cone–type visual system (*A*), and avian violet cone–type visual system (*B*; sensitivity curves from Endler and Mielke 2005). The short-wavelength chromatic minimum for the ultraviolet–cone type visual system is 417 nm (*A*), whereas it is 454 nm for the violet cone–type visual system (*B*). The wavelengths of chromatic minimum (marked with an asterisk) in each of these visual systems are perceived as fully chromatic by the other type of visual system.

homogenizing effect inherent in Fechner's law is an accurate description of the neural mechanisms by which multiple cone stimuli are resolved into a singular color perception.

In conclusion, the Goldsmith (1990) color space utilized in this study provides a quantitative, tetrahedral map of avian color perception that is easy to calculate, pragmatic, heuristic, and quantitatively precise. The sensory space proposed by Endler and Mielke (2005) requires measurements of ambient light variation from the appropriate environments, but it does not provide any additional empirical advantages. We advocate broad application of Goldsmith's (1990) color space in future analyses of integumentary color evolution, signaling, and perception in tetrachromatic vertebrates and other organisms.

Spectral vs. Color Space Descriptions

The vast majority of current literature on the ecology and evolution of avian plumage coloration is based on the direct analysis of reflectance spectra (Hill and McGraw 2006*a*, 2006*b*). Because reflectance spectra are continuous functions with a diversity of shapes (e.g., fig. 2), none of the traditional definitions of hue or chroma (recently reviewed by Montgomerie 2006) function logically across the wide variety of reflectance spectra produced by various structural and pigmentary mechanisms. This limitation creates an obvious constraint to comparative analysis of color evolution. In contrast, a tetrachromatic color space provides a heuristic and highly comparable alternative to the traditional array of methods used to analyze avian reflectance spectra. Analyses of the physics and biochem-

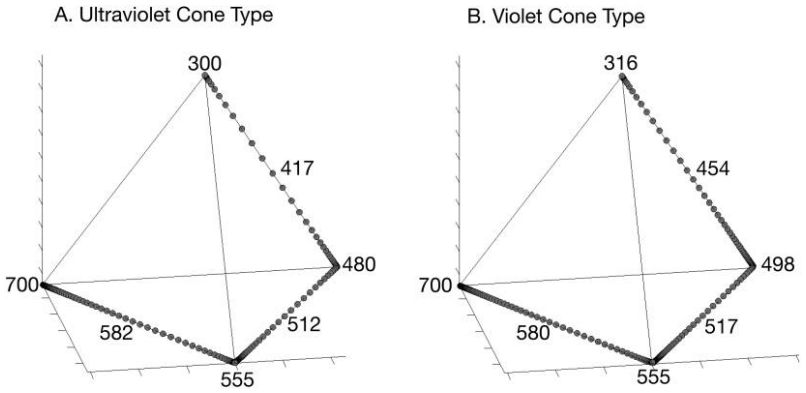

Figure 9: Tetrahedral plot of color points for monochromatic illumination across the avian visible spectrum from 300 to 700 nm in the avian UV cone–type visual system (*A*) and avian violet cone–type visual system (*B*); sensitivity curves from Endler and Mielke (2005). The wavelengths labeled are for the vertices and the chromatic minima (see fig. 8), which are positioned along an edge of the tetrahedron between vertices. The two types of avian visual systems differ principally in the mapping of shorter, nonultraviolet, visible wavelengths (400–500 nm) into the tetrahedral color space.

istry of avian color production should continue to be conducted with the reflectance spectra themselves, because their form can be used to test physical and molecular hypotheses (e.g., Prum et al. 1999; Prum and Torres 2003; Prum 2006). But redefining the fundamental color variables of hue and chroma in the context of the tetrahedral avian color space has many advantages for studying the function and evolution of avian crypsis, communication, social behavior, and their evolution. Tetrachromatic color analysis should become fundamental to comparative, ethological, and evolutionary research in avian color signals.

PCA of reflectance spectra has already been used to mitigate some of the limitations of traditional analysis of plumage reflectance spectra. PCA can quantify a diverse sample of reflectance spectra, but it has many other limitations (Vorobyev et al. 1998; Endler and Mielke 2005; Endler et al. 2005). Most importantly for comparative behavioral and evolutionary biology, principal components axes are unique to each sample of analysis and do not provide a standardized, generalizable, and transportable scale of measurement that can be compared among independent analyses. Identifying the scale of any quantitative representation of data is a fundamental aspect of any measurement procedure (Hand 2004). Although PCA succeeds as a quantitative representation of spectral data, it fails to provide a pragmatic, generalizable scale of variation that would permit cumulative advance in our understanding of color variation among birds. The tetrahedral color space used here provides a physiologically realistic and generalizable framework for the description and comparative analysis of the diversity of avian plumage colors.

Chroma in a Tetrahedral Visual System

If chroma is related to the distance of a color point from the achromatic origin, then different hues necessarily have different possible maximum chroma. This generalizable result is a biological consequence of the shape and distribution of cone sensitivity functions (Hurvich 1981). Following analyses for human vision (Hurvich 1981), the distribution of chroma for pure spectrum colors in avian visual systems shows three wavelengths of minimum chromatic experience, or "troughs" in the curve (fig. 8). Interestingly, the positions of these chromatic minima between the avian UV and violet cone–type visual systems differ markedly only for the lowest wavelength of chromatic minimum—417 nm for the UV cone type (fig. 8*A*) but 454 nm for the violet cone type (fig. 8*B*). These spectral chroma functions are so dynamic that the smaller wavelength chromatic minima in each visual system (417 and 453 nm, respectively) have maximal chroma in the alternative visual system (see asterisks in fig. 8). Birds with the UV cone type also have a broader gap between the two shorter-wavelength chromatic minima (95 nm) than do birds with the violet cone type (63 nm). The specific wavelengths of each chromatic minimum are the result of variations in how the cone sensitivity functions map the monochromatic spectrum into the tetrahedral color space (fig. 9; see also Goldsmith 1990, their fig. 28; Vorobyev et al. 1998, their fig. 4).

Although pure monochromatic colors do not exist in nature, these results demonstrate that chroma cannot be meaningfully defined as a function of the shape of the reflectance spectrum alone, as is commonly done (Montgomerie 2006). By any spectral definition of chroma, spec-

tra of similar shapes including pure spectrum colors would be equivalently chromatic. To organisms, however, certain wavelengths necessarily appear less saturated than others. Just as "pure" turquoise and yellow colors appear to humans to be closer to white than do "pure" blue, green, or red (Hurvich 1981), some hues will appear to birds to have a greater inherent whiteness or lightness. This information is fundamental to chromatic experience but is unavailable in a reflectance spectrum.

Interestingly, birds with different visual systems perceive chroma differently. Previous comparisons of avian UV- and violet-cone vision systems have emphasized the importance of differences in the peaks of their cone sensitivity functions (Vorobyev et al. 1998; Hart 2001; Vorobyev 2003; Hart and Vorobyev 2005). However, the distributions of most color points in the tetrahedral color spaces of birds with UV and violet cone types are surprisingly similar (Endler et al. 2005; M. C. Stoddard and R. O. Prum, unpublished data). We hypothesize that the differences in the distribution of chromatic perception among different wavelengths between the UV and violet cone–type visual systems (figs. 8, 9) may be a more important target for natural selection on opsin absorbance than the peak sensitivities themselves. Both UV and violet cone types are at the short-wavelength end of the avian visible spectrum, and both lack carotenoids in the cone oil droplets. Both cone types have similar, unfiltered, open-ended sensitivities into the near ultraviolet. Thus, the evolution of chromatic perception may have been more important in the differentiation and maintenance of the UV and violet cone types in birds than their differences in peak of spectral sensitivity per se. Avian cone sensitivities may have evolved through natural selection on the map of wavelengths between 300 and 490 nm to the vertices and edges of their color space rather than on the breadth of sensitivity in the UV.

Future investigations of avian UV/violet cone evolution should examine this hypothesis. For example, one of its predictions is that birds with UV or violet cone types should evolve ultraviolet plumage signals with equal frequency. Initial confirmation of this prediction comes from the high frequency of intraspecific color signals with predominantly ultraviolet reflectance in birds with violet cones. Structural colors with peak reflectances far below 400 nm have evolved in numerous avian lineages with violet as well as UV cone types (e.g., in Galliformes and suboscine passerines; Prum 2006; Prum and Torres 2003).

Note Added in Proof

A recent, more comprehensive phylogeny of the Cardinalidae by Klicka et al. (2007) places the monotypic cardinalid genus *Cyanoloxia* and the three species of the formerly emberizid genus *Amaurospiza* within the genus *Cyanocompsa*. The steely blue *Cyanoloxia glaucocaerulea* is placed as the sister species to *Cyanocompsa brissoni*, and the blackish and deep blue *Amaurospiza concolor* is placed as the sister group to the clade of *Cyanocompsa cyanoides*, *C. brissoni*, and *C. glaucocaerulea*. *Passerina cyanea* is also placed as the sister group to the *Passerina caerulea–Passerina amoena* clade but without significant support. The addition of the deep blue and blackish colors of the *Cyanoloxia* and *Amaurospiza* species to the *Cyanocompsa* clade are generally congruent with the phylogenetic patterns documented from the more exclusive sample analyzed here, including the derived colonization of new regions of the color space and color volume expansion in the *P. caerulea–P. amoena* and the painted clades within *Passerina*. Further, the new phylogenetic hypothesis supports a single evolutionary origin of blue structural barb coloration within the Cardinalidae in the common ancestor of this clade.

Acknowledgments

We thank the American Museum of Natural History, New York, and the Yale Peabody Museum, New Haven, Connecticut, for research access to their bird specimens. The research was supported by a Yale Peabody Museum Summer Research Fellowship to M.C.S. and by Yale University research funds to R.O.P. We thank A. Badyaev, J. Endler, T. Goldsmith, and G. P. Wagner for stimulating discussions and technical suggestions. J. Endler kindly shared forthcoming manuscripts. The manuscript was improved by comments from four anonymous reviewers, O. Håstad, and J. Marshall. We also thank N. and R. Bowers, J. Culbertson, E. Endrigo, M. Grosselet, P. LaTourette, G. McElroy, J. Ownby, G. Ruiz, D. Wechsler, and the Visual Resources for Ornithology avian photo library for permission to reproduce their photographs of *Cyanocompsa* and *Passerina* buntings (fig. 2).

Literature Cited

Burkhardt, D. 1989. UV vision: a bird's eye view of feathers. Journal of Comparative Physiology A 164:787–796.

Cuthill, I. C. 2006. Color perception. Pages 3–40 *in* G. E. Hill and K. J. McGraw, eds. Bird coloration. Vol. I. Mechanisms and measurements. Harvard University Press, Cambridge, MA.

Cuthill, I. C., A. T. D. Bennett, J. C. Partridge, and E. J. Maier. 1999. Plumage reflectance and the objective assessment of avian sexual dichromatism. American Naturalist 160:183–200.

Eaton, M. D. 2005. Human vision fails to distinguish widespread sexual dichromatism among sexually "monogamous" birds. Proceedings of the National Academy of Sciences of the USA 102: 10942–10946.

Eaton, M. D., and S. M. Lanyon. 2003. The ubiquity of avian ultra-

violet plumage reflectance. Proceedings of the Royal Society B: Biological Sciences 270:1721–1726.

Endler, J. A. 1993. The color of light in forests and its implications. Ecological Monographs 61:1–27.

Endler, J. A., and A. L. Basolo. 1998. Sensory ecology, receiver biases and sexual selection. Trends in Ecology & Evolution 13:415–420.

Endler, J. A., and P. W. J. Mielke. 2005. Comparing entire colour patterns as birds see them. Biological Journal of the Linnean Society 86:405–431.

Endler, J. A., and M. Théry. 1996. Interacting effects of lek placement, display behavior, ambient light, and color patterns in three Neotropical forest-dwelling birds. American Naturalist 148:421–452.

Endler, J. A., D. A. Wescott, J. R. Madden, and T. Tobson. 2005. Animal visual systems and the evolution of color patterns: sensory processing illuminates signal evolution. Evolution 59:1795–1818.

Felsenstein, J. 1985. Phylogenies and the comparative method. American Naturalist 125:1–15

Freckleton, R. P., P. H. Harvey, and M. Pagel. 2002. Phylogenetic analysis and comparative data: a test and review of evidence. American Naturalist 160:712–726.

Goldsmith, T. H. 1990. Optimization, constraint, and history in the evolution of eyes. Quarterly Review of Biology 65:281–322.

Goldsmith, T. H., and B. K. Butler. 2005. Color vision of the budgerigar (*Melopsittacus undulatus*): hue matches, tetrachromacy, and intensity discrimination. Journal of Comparative Physiology A 191: 933–951.

Hand, D. J. 2004. Measurement theory and practice. Arnold, London.

Hart, N. S. 2001. The visual ecology of avian photoreceptors. Progress in Retinal and Eye Research 20:675–703.

Hart, N. S., and M. Vorobyev. 2005. Modelling oil droplet absorption spectra and spectral sensitivities of bird cone photoreceptors. Journal of Comparative Physiology A 191:381–392.

Heindl, M., and H. Winkler. 2003. Interacting effects of ambient light and plumage color patterns in displaying wire-tailed manakins (Aves, Pipridae). Behavioral Ecology and Sociobiology 53:153–162.

Hill, G. E., and K. J. McGraw, eds. 2006*a*. Bird coloration. Vol. 1. Mechanisms and measurement. Harvard University Press, Cambridge, MA.

———. 2006*b*. Bird coloration. Vol. 2. Function and evolution. Harvard University Press, Cambridge, MA.

Hurvich, L. M. 1981. Color vision. Sinauer, Sunderland, MA.

Kelber, A., M. Vorobyev, and D. Osorio. 2003. Animal colour vision: behavioural tests and physiological concepts. Biological Review 78: 81–118.

Klicka, J., A. J. Fry, R. M. Zink, and C. W. Thompson. 2001. A cytochrome-*b* perspective on *Passerina* bunting relationships. Auk 118:611–623.

Klicka, J., K. Burns, and G. M. Spellman. 2007. Defining a monophyletic Cardinalini: a molecular perspective. Molecular Phylogenetics and Evolution 45:1014–1032.

Kuehni, R. G. 2003. Color space and its divisions. Wiley, Hoboken, NJ.

Maddison, W. P., and D. R. Maddison. 2000. MacClade 4.0. Sinauer, Sunderland, MA.

Martins, E. P., and T. F. Hansen. 1997. Phylogenies and the comparative method: a general approach to incorporating phylogenetic information into the analysis of interspecific data. American Naturalist 149:646–667.

Montgomerie, R. 2006. Analyzing colors. Pages 90–147 *in* G. E. Hill and K. J. McGraw, eds. Bird coloration. Vol. 1. Mechanisms and measurements. Harvard University Press, Cambridge, MA.

Müller, G. B., and G. P. Wagner. 1991. Novelty in evolution: restructuring the concept. Annual Review of Ecology and Systematics 22: 229–256.

Ödeen, A., and O. Håstad. 2003. Complex distribution of avian color vision systems revealed by sequencing the SWS1 opsin from total DNA. Molecular Biology and Evolution 20:855–861.

Pagel, M. 1997. Inferring evolutionary process from phylogenies. Zoologica Scripta 26:331–348.

———. 1999. Inferring the historical patterns of biological evolution. Nature 401:877–884.

Prum, R. O. 1997. Phylogenetic tests of alternative intersexual selection mechanisms: macroevolution of male traits in a polygynous clade (Aves: Pipridae). American Naturalist 149:668–692.

———. 2006. Anatomy, physics, and evolution of avian structural colors. Pages 295–353 *in* G. E. Hill and K. J. McGraw, eds. Bird coloration. Vol. 1. Mechanisms and measurements. Harvard University Press, Cambridge, MA.

Prum, R. O., and R. H. Torres. 2003. Structural colouration of avian skin: convergent evolution of coherently scattering dermal collagen arrays. Journal of Experimental Biology 206:2409–2429.

Prum, R. O., R. H. Torres, S. Williamson, and J. Dyck. 1999. Two-dimensional Fourier analysis of the spongy medullary keratin of structurally coloured feather barbs. Proceedings of the Royal Society B: Biological Sciences 266:13–22.

Prum, R. O., S. Andersson, and R. H. Torres. 2003. Coherent scattering of ultraviolet light by avian feather barbs. Auk 120:163–170.

Vorobyev, M. 2003. Coloured oil droplets enhance colour discrimination. Proceedings of the Royal Society B: Biological Sciences 270:1255–1261.

Vorobyev, M., and D. Osorio. 1998. Receptor noise as a determinant of colour thresholds. Proceedings of the Royal Society B: Biological Sciences 265:351–358.

Vorobyev, M., D. Osorio, A. T. D. Bennett, N. J. Marshall, and I. C. Cuthill. 1998. Tetrachromacy, oil droplets and bird plumage colours. Journal of Comparative Physiology A 183:621–633.

Vorobyev, M., J. Marshall, D. Osorio, N. Hempel de Ibarra, and R. Menzel. 2001. Colourful objects through animal eyes. Color Research and Application 26(suppl.):S214–S217.

West, G., and M. H. Brill. 1982. Necessary and sufficient conditions for Von Kries chromatic adaptation to give color constancy. Journal of Mathematical Biology 15:249–258.

Associate Editor and Editor: Monica A. Geber

DOI: 10.1086/587526

Appendix from M. C. Stoddard and R. O. Prum, "Evolution of Avian Plumage Color in a Tetrahedral Color Space: A Phylogenetic Analysis of New World Buntings"

(Am. Nat., vol. 171, no. 6, p. 755)

Supplementary Methods and Analyses

Detailed Methods

Plumage Color Measurement

We measured the reflectance spectra of plumage patches of males of all species in the genera *Cyanocompsa* (three species) and *Passerina* (seven species; Cardinalidae). This small clade was selected because these species exhibit rich and varied color patterns and because a robust phylogenetic analysis exists for the clade (Klicka et al. 2001). We measured color patches on 10 mature adult male representatives for each species, using study skins from the Yale Peabody Museum of Natural History, New Haven, Connecticut, and the American Museum of Natural History, New York. Specimens with obvious delayed plumage maturation or fading were avoided. For each species, reflectance spectra were measured from six standard plumage patches: crown, back, rump, throat, breast, and belly. Reflectance spectra were measured three times per patch per individual. Additional color patches were also measured for certain species if they had additional colors that were distinct to the human eye. Depending on the species, the additional color patches were the forehead, epaulet, cheek, wing bar, lower belly, and nape. Most species had no additional color patches, although others had as many as three.

The reflectance spectra of color patches were measured using an Ocean Optics S2000 spectrometer with an Ocean Optics DH-2000-BAL deuterium-halogen light source. The spectrometer generated 2,048 reflectance data points between 178 and 879 nm and 1,141 points between 300 and 700 nm. Measurements were relative to a standard white Spectralon tablet from Ocean Optics. The dark reference was the ambient light of a darkened room. Measurements were taken with perpendicular incident light from ~6 mm from the plumage, which provided an illumination field of ~3 mm^2 (Prum et al. 1999, 2003). The reflectance probe was held in an aluminum block that was held next to the plumage to obscure ambient light during measurement. Integration time was 500 ms. Percent reflectance ($\%R$) was calculated as $\%R = [(S - D)/(W - D)] \times 100$, where S is reflectance of specimen, D is reflectance of the dark standard, and W is reflectance of the white standard.

For the comparative analyses, the average reflectance of each patch for each species was calculated by computing the specimen averages from the three replicate spectra measured for each individual for each data point between 300 and 700 nm and then averaging the 10 specimen spectra to obtain the species reflectance spectra for the patch. Analyses of individual variation are described below.

Tetrahedral Color Space

We developed a computer program—TETRACOLORSPACE—for the tetrahedral analysis of avian reflectance spectra, using MATLAB 7 software (MathWorks, Natick, MA). The program performs all of the tetrahedral analyses conducted in this article. MATLAB .m files are available on request from the authors or at http://www.yale.edu/eeb/prum/.

To estimate the stimulation of each color cone type $\{u\ s\ m\ l\}$, following Goldsmith (1990), we calculated the idealized stimulus, Q_I, of each color cone type by the reflectance spectrum of a plumage patch:

$$Q_I = \int_{300}^{700} R(\lambda)C_r(\lambda)d\lambda, \tag{A1}$$

where $R(\lambda)$ is the reflectance spectrum of the plumage patch and $C_r(\lambda)$ is the spectral sensitivity function of each cone type r. We normalized both the $R(\lambda)$ and $C_r(\lambda)$ functions to have to integrals of 1. Stimulus Q_l is equivalent to Q_r of Endler and Mielke (2005; their eq. [4]) but with the further extension of their simplifying assumption about the transmission spectrum and the veiling light to the ambient light. Following Goldsmith (1990), we treat the irradiance spectrum $I(\lambda)$ as a constant across all visible wavelengths, with an integral equal to 1.

Spectral sensitivity functions, $C_r(\lambda)$, have not been measured for *Cyanocompsa*, *Passerina*, or any other emberizoid bird. Spectral sensitivity appears to be relatively uniform among higher oscine birds (Hart 2001), which share the UVS cone type that is characterized by a peak absorbance in the ultraviolet (Ödeen and Håstad 2003). Consequently, we used average spectral sensitivity curves of an ultraviolet cone–type retina from Endler and Mielke (2005, supplementary online materials). TETRACOLORSPACE can analyze spectra using either violet- or ultraviolet-sensitive cone types from Endler and Mielke (2005).

Several orientations for tetrahedral color spaces have been proposed (Burkhardt 1989; Goldsmith 1990; Kelber et al. 2003), but we used the geometry defined by Endler and Mielke (2005), which places the achromatic point of equal cone stimulation (i.e., white, black, or gray) at the origin of a Cartesian coordinate system and the UVS, or u (or VS, v), vertex along the vertical Z-axis (fig. 1). The relative stimulation $\{u\ s\ m\ l\}$ data for any color can be converted to a color point in the tetrahedral color space with the Cartesian coordinates X, Y, and Z by the equations (Endler and Mielke 2005)

$$\begin{aligned} X &= \frac{1 - 2s - m - u}{2}\sqrt{\frac{3}{2}}, \\ Y &= \frac{-1 + 3m + u}{2\sqrt{2}}, \\ Z &= u - \frac{1}{4}. \end{aligned} \tag{A2}$$

The Cartesian (X, Y, Z) coordinates of each color point were then converted to its spherical coordinates—θ, ϕ, and r—that define the color vector (fig. 1). For each species, the color vectors of all plumage patches were plotted as points in the tetrahedral color space. The advantage of using spherical coordinates is that position of the color point is described in terms of three meaningful quantities rather than the X, Y, Z coordinates, which are only an arbitrary frame of reference for the tetrahedron. The angles θ and ϕ define the hue, or direction, of the color vector. Because of the orientation of the tetrahedron, θ is the trichromatic $\{s\ m\ l\}$ or RGB (red, green, blue) component of hue, and ϕ is the exclusively ultraviolet or violet component of hue. Coordinate r is the chroma, or the distance of the color point from the achromatic origin.

Conversion of color points from a tetrachromatic color space into an analogous trichromatic color area that lacks the ultraviolet sensory dimension cannot be accomplished by merely viewing the tetrahedron from the Z-axis (e.g., Endler et al. 2005, their fig. 3), or flattening the three-dimensional color space into a plane. Rather, new tristimulus $\{s, m, l\}$ values must be renormalized to their sum alone. Mathematically, this is the equivalent of projecting down from any color point onto the base of the tetrahedron along the line that travels from the u vertex through that color point. TETRACOLORSPACE can do these transformations for comparing trichromatic and tetrachromatic visualization.

Hue

Hue is defined as the direction of the color vector and is given by angles θ and ϕ, which are analogous to the longitude and latitude, respectively, of any point in the color space (fig. 1). The azimuth angle θ, or longitude, is the angular displacement of the color vector from the positive X-axis, which runs between the s (blue) and m (green) vertices (fig. 1). The elevation angle ϕ, or latitude, is the angular displacement of the color vector from the horizontal X-Y plane (fig. 1). The chroma, or saturation, of a color is given by the magnitude of r, or its distance from the achromatic point at the origin. Colors of the same hue that differ in chroma are distributed on a line at different lengths from the origin.

Because the ultraviolet vertex is oriented along the Z-axis, θ describes the purely trichromatic $\{s\ m\ l\}$

component of the hue in the horizontal plane. The elevation angle ϕ describes the exclusive contribution of ultraviolet/violet stimulation to the hue. Thus, ϕ constitutes a measure of the ultraviolet/violet component of hue. It is not identical to percent UV or violet reflectance (i.e., the Cartesian Z coordinate), because ϕ contains only information about the direction of the color vector, and colors of the same hue with different chroma can vary extensively in the relative stimulation of the UVS cone. Following Endler et al. (2005), we used the two-dimensional Robinson projection function in MATLAB to visualize variation in hue within a plumage independent of variation in chroma.

Chroma

Chroma r is defined as the magnitude or distance of a color point from the achromatic origin, or the length of the color vector. Because the color space is a tetrahedron and not a sphere, different hues vary in their maximum chroma, r_{max}. The four pure hues that extend from the origin toward the vertices of the tetrahedron have $r_{max} = 0.75$. All other hues have a smaller maximum chroma because a hue vector of $r = 0.75$ would extend beyond the boundaries of the color space. Equations for r_{max} for any given hue, θ, and ϕ, are presented in "Functions of Cone Stimulation for a Given Hue" and "Maximum Chroma."

In many contexts, it may be more informative to define the chroma of a color relative to the maximum chroma for its hue rather than to its absolute difference from achromatic ($r = 0$), or the maximum chroma of a pure hue ($r = 0.75$). Consequently, for each plumage patch, we calculated the achieved chroma, or r_A, which is the proportion of maximum possible chroma for its hue, or r/r_{max}.

Measures in Color Space

For each plumage, we computed the average color span, which is the average of the Euclidean distances between each pair of colors in the plumage (Δ_T of Endler and Mielke [2005]) and the variance in the color span. Average color span is a measure of overall color contrast among the patches in the plumage, and color span variance measures the uniformity of the color contrast within the plumage.

We estimated the volume of the color space occupied by the color patches of each plumage by calculating the volume of the minimum convex polygon that contains all the color points of the plumage. We used the CONVHULLN command in MATLAB. (Endler et al. [2005] report color volumes but do not document their method for calculating them.) Plumage color volume is a measure of diversity in color within a plumage. Unlike span, color volume captures the three-dimensional breadth of color space occupancy.

We developed a new measure of contrast in hue that is independent of chroma. Hue disparity α is the magnitude of the angle between two color vectors. We calculated α by

$$\cos\alpha = \cos(\phi_1)\cos(\phi_2)\cos(\phi_1 - \phi_2) + \sin(\phi_1)\sin(\phi_2), \tag{A3}$$

where ϕ_1 and θ_1 and ϕ_2 and θ_2 are the spherical azimuth and elevation angles for any two color vectors, respectively. (Alternatively, $\cos\alpha$ can be calculated from the scalar product of the two corresponding direction vectors.)

Hue disparity can be understood in terms of color complementarity. Complementary colors have maximum hue disparity, $\alpha = \pi$. Alternatively, hue complementarity can be defined as α/π and reported on a proportional scale of 0 (identical) to 1 (complementary). We calculated the average hue disparity of all patches in each plumage, which gives a measure of overall hue contrast within a plumage. We also calculated the variance in hue disparity, which is a measure of the uniformity of hue contrast among plumage patches.

The plumages of *Cyanocompsa brissonii* and *Cyanocompsa cyanoides* include multiple, very dark, blackish plumage patches (figs. 2*A*–2*C*, 3*A*). Our preliminary analyses documented that these blackish patches have so little reflectance that noise in these spectra can produce random colors (fig. 3*A*). These random colors created spurious measurements of span, volume, hue disparity, and chroma for these species. Consequently, we restricted the color space analyses to those five patches (*C. brissonii*) and four patches (*C. cyanoides*) with ≥0.05 normalized brilliance (table 1).

Brilliance

Brilliance is processed independently from color (Goldsmith 1990; Hart 2001; Kelber et al. 2003; Vorobyev and Osorio 1998) and therefore is not analyzed using the color space. For each color patch, we averaged the

reflectance values for each 1-nm window between 300 and 700 nm. We measured peak percent reflectance (intensity), the wavelength λ_{max} of maximum reflectance, and normalized brilliance (total reflectance)/(100 × N), where total reflectance is the sum of percent reflectance at all data points between 300 and 700 nm and N is the number of data points between 300 and 700 nm ($N = 401$). In addition, we calculated the average percent UV reflectance (average u) of each plumage, which is a measure of the ultraviolet contribution to plumage color.

Comparing Color Spaces

We compared our application of Goldsmith's (1990) tetrahedral color space to Endler and Mielke's (2005) method for two representative species—*Cyanocompsa parellina* and *Passerina ciris*—under three different ambient light spectra. We repeated Endler and Mielke (2005) in calculating

$$Q_r = \int_{300}^{700} R(\lambda)\, I(\lambda) C_r(\lambda)\, d\lambda, \tag{A4}$$

where $R(\lambda)$ is the reflectance spectrum of the plumage patch, $I(\lambda)$ is the ambient irradiance spectrum, and $C_r(\lambda)$ is the spectral sensitivity function of each cone type r, assuming perfect transmission and no veiling light.

We then calculated q_r of Endler and Mielke (2005) by performing the von Kries transformation for achieving color constancy:

$$q_r = \frac{\int_{300}^{700} R(\lambda)\, I(\lambda) C_r(\lambda)\, d\lambda}{\int_{300}^{700} I(\lambda) C_r(\lambda)\, d\lambda}\ . \tag{A5}$$

The von Kries transformation normalizes the quantal catch estimate of each cone channel by dividing it by the quantity of stimulation of a flat, achromatic spectrum under the ambient light. Finally, following Fechner's law (Vorobyev et al. 1998; Kuehni 2003; Endler and Mielke 2005, eq. [10]), the q_r values were then log transformed before normalizing to a sum of 1, producing $\{u\ s\ m\ l\}$ values of signaler sensory experience to plot in tetrahedral color space. Irradiance spectra were collected with an Ocean Optics spectrophotometer using a cosine corrector, under typical forest cloudy, interior forest shade, and forest sunny-gap conditions in Amazonian Brazilian lowland humid rainforest (courtesy of M. Anciães).

To understand the cumulative effects of each transformation, we generated normalized $\{u\ s\ m\ l\}$ and the corresponding θ, ϕ, and r values based on Q_r, q_r, and log-transformed q_r values sequentially. We then compared the tetrachromatic color variables for individual patches and for entire plumages for both species.

Note that the magnitudes of the q_r quantal catch estimates (which are unitless) are particularly sensitive to the magnitude of reflectance values because $R(\lambda)$ appears only in the numerator (eq. [A5]). We haven chosen the least arbitrary values and normalized all the input functions to integrals of 1, which produces very small values of q_r. Under these conditions, log transformation was found to have very dramatic and unpredictable effects (see "Results"). It may be possible to mitigate the distorting effects of log transformation of the quantal catch estimates by manipulating the scale of the variation of the input functions to eq. [A5], particularly $R(\lambda)$. Nevertheless, the effect of log transformation of the quantal catch estimates remains problematic.

Comparative Phylogenetic Analyses

We examined the phylogenetic history of the evolution of color using the best-fit maximum-likelihood phylogenies of *Cyanocompsa* and *Passerina* by Klicka et al. (2001), which were based on sequencing of the mitochondrial cytochrome *b* gene in all species of the clade. In the maximum-likelihood phylogeny of the clade (Klicka et al. 2001), *Cyanocompsa* and *Passerina* are monophyletic sister taxa (fig. 6). Within *Cyanocompsa*, *brissonii* and *cyanoides* form a clade, with *C. parellina* as their sister group (fig. 6). Within *Passerina*, *cyanea* is the basal lineage, and the remaining six species form two clades. The first includes *Passerina caerulea* and *Passerina amoena* (fig. 6). The second, which we refer to as the "painted" clade, consists of *Passerina rositae* and *Passerina leclancherii* as the successive sister groups to a *Passerina versicolor* and *P. ciris* clade (fig. 6).

First, we examined patterns in the variation of continuous color characters using the linear parsimony algorithm in the MacClade 4.0 (Maddison and Maddison 2000) computer program. Second, we used the program

CONTINUOUS 1.0d13 (Pagel 1997, 1999) to investigate and compare alternative evolutionary models for the phylogenetic variation in color of the *Passerina* and *Cyanocompsa* clades. CONTINUOUS applies a generalized least squares (GLS) method to the phylogenetic analysis of continuous character data (Martins and Hansen 1997; Pagel 1997, 1999). In a GLS model, the value of the trait y observed in the ith species, y_i, is given by

$$y_i = \alpha + \beta\Sigma t_i + e_i, \tag{A6}$$

where α is the y-intercept of the regression of y (i.e., the ancestral value of y within the clade), β is the slope of the regression of y with evolutionary time or genetic distance, Σt_i is the sum of the evolutionary time or the genetic distance on all the branches leading to species i, and e_i is a random error term. Estimation of α and β requires accounting for the shared phylogenetic history, or phylogenetic covariance, between trait values of different species, using a matrix of shared evolutionary distances among species. The values of α and β are estimated using a GLS procedure (Pagel 1997, 1999). The goodness of fit of alternative evolutionary models to the data and the phylogeny are compared using the likelihood ratio test (Pagel 1997, 1999).

In CONTINUOUS, a simple evolutionary model can also be altered using three other scaling, or weighting, parameters that are equivalent to different assumptions about the tempo of evolution or the strength of phylogenetic association among lineages (Pagel 1997, 1999; Freckleton et al. 2002). The parameter κ stretches or compresses the effects of individual branch lengths. A value of $\kappa > 1$ stretches long branches more than shorter ones, and a value of $\kappa = 0$ corresponds to the punctuated-equilibrium mode of evolution, with bursts of change only at each speciation event. The parameter δ adjusts the rate of trait evolution over time or distance. A value of $\delta < 1$ decreases the rate of change over evolutionary time, and a value of $\delta > 1$ increases the rate of change over evolutionary time. The parameter λ weights the importance of the phylogenetic correlation among species. A default value of $\lambda = 1$ corresponds to a strictly phylogenetic evolutionary model, and a value of $\lambda = 0$ corresponds to a complete lack of phylogenetic correlation among the species values, or a "star" phylogeny. CONTINUOUS will use default values of κ, δ, and $\lambda = 1$, user input values, or maximum likelihood estimates of up to two of the three parameters based on the fit to the data.

We used the phylogeny and genetic distances from Klicka et al. (2001, their fig. 2*a*) to specify the tree topology and branch lengths in our analyses. We compared the log likelihoods of various alternative evolutionary models of the variation among 10 in-group species for eight plumage color variables: average color span, span variance, plumage color volume, hue disparity, the variance in hue disparity, average chromaticity, maximum chromaticity, and average brilliance.

Functions of Cone Stimulation for a Given Hue

Hue—the direction of the color vector—is determined by the proportions, or ratios, of the differences in stimulation among the four color channels. A given hue does not have a unique combination of relative stimulation $\{u\ s\ m\ l\}$ values. Rather, there are infinite $\{u\ s\ m\ l\}$ combinations that will produce a given hue. Points along any straight line from the achromatic origin share the same hue; only the chroma, or the magnitude of the color vector, is changing.

Here, we present a set of four functions that describe how stimulation of the four color channels—ultraviolet or violet (u), short wavelength (s), medium wavelength (m), and long wavelength (l)—varies as a function of chroma r for any given hue, θ and ϕ. These functions are

$$u(r) = r\cos(\alpha_{h/u}), \tag{A7}$$

$$s(r) = r\cos(\alpha_{h/s}), \tag{A8}$$

$$m(r) = r\cos(\alpha_{h/m}), \tag{A9}$$

$$l(r) = r\cos(\alpha_{h/l}), \tag{A10}$$

where α is the hue disparity angle between the hue vector (h) and each of the vertex vectors u, s, m, and l, which extend from the achromatic origin to each vertex of the tetrahedron. The value of α is calculated using equation (A3).

Each hue is characterized by a unique combination of four functions for the relative reflectance or stimulation

of each color channel over variation in chroma, r (e.g., fig. A1). At the achromatic origin ($r = 0$), all vectors have equivalent reflectance, or stimulation, among all four channels. As r increases, the stimulation of each cone changes linearly by the slope of cos α (fig. A1). The slopes of the four functions sum to 0 because the sum of the four channel values remains equal to 1.

Maximum Chroma

To determine the maximum possible chroma r_{max} for any hue, we identify α_{max}, the largest of the angles formed between the hue vector and the $\{u\ s\ m\ l\}$ vertex vectors. Angle α_{max} is always the angle between the hue vector and the vertex vector opposite the side of the tetrahedron through which the hue vector points. Using geometry,

$$r_{max} = \frac{0.25}{\cos(\pi - \alpha_{max})}. \tag{A11}$$

For a given hue, r_{max} is the r value at which the cone channel with the most negative slope equals 0 (fig. A1). Thus, the functions for relative stimulation versus chroma only apply only over the domain of $r = 0$ to r_{max}.

For example, the orange-yellow breast of *Passerina leclancherii* (fig. 2*H*) has a chroma, r, of 0.40 that is only 53% of the maximum chroma of a pure hue ($r_{max} = 0.75$), but it has an achieved chroma that is 93% of the maximum chroma for its hue ($r_{max} = 0.43$; fig. A1).

Analysis of Intraspecific Variation

We analyzed individual variation in two representative species—*Cyanocompsa parellina* and *Passerina ciris*—using two methods. In the first analysis, we examined the variation among the tetrahedral color vectors derived from the reflectance spectra of patches of 10 male specimens. For each patch in each species, we characterized the individual variation in the color points using several measures: the variance in span between each individual plumage color point and the average color point (i.e., the centroid), the color volume of the individual plumage points, the average span, the hue disparity, and achieved chroma of the replicate spectra.

The variances in the span between color points from spectra of the 10 individuals and their average point, or centroid, for each plumage patch were very small ($\sim 10^{-4}$–10^{-3}) for both *C. parellina* and *P. ciris* (data not shown). The average spans of the individual color points in both species were also small ($\sim 10^{-2}$). These values do rival the average span of the whole plumages of *Cyanocompsa* and *Passerina cyanea* (table 2), but this result is because the plumages of these species consist essentially of replicate patches of a single color. The volumes of the color points for each patch of the 10 individuals were very small (10^{-6}–10^{-4} for both species), again similar to the volumes for the monochromatic plumages of *Cyanocompsa* and *P. cyanea*.

A second analysis was performed by calculating the plumage color diversity measures (table 2) separately for each of 10 individuals for *C. parellina* and *P. ciris*. For both species, the averages of the color diversity measures calculated from the individual males were virtually identical to the color diversity measures, based on the average spectra from the 10 males (data not shown).

In conclusion, both analyses of variation in the hue and chroma of individual spectra support the accuracy of the tetrachromatic analyses of the average spectra. Further, it is clear that the TETRACOLORSPACE tool is appropriate for quantitative analysis of individual variation in plumage coloration.

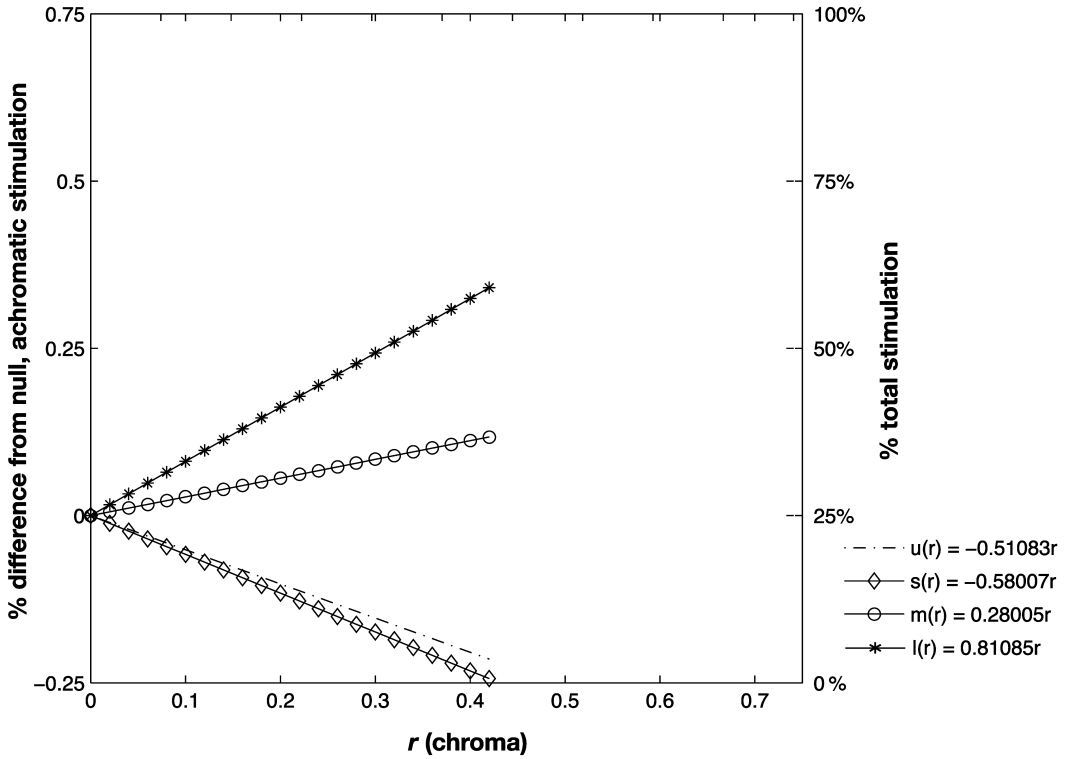

Figure A1: Functions for relative reflectance/stimulation of the *u*, *s*, *m*, and *l* channels with changes in *r*, or chroma, for the hue of the orange breast of *Passerina leclancherii* (fig. 2*H*). Quantity *r* is the length of the color vector. The percent stimulation of each channel is given by two scales, relative to null achromatic stimulation (*left axis*; −0.25 to 0.75) and percent total stimulation (*right axis*; 0 to 1). The sum of the slopes of the four functions (*right*) is 0 (see "Functions of Cone Simulation for a Given Hue"). The maximum achievable chroma for any hue occurs when cone function with the most negative slope—in this case, *s*(*r*)—intersects the *X*-axis (see "Maximum Chroma"). The maximum achievable chroma for this orange hue is 0.43, but the observed chroma is 0.40. Thus, the achieved chroma of this orange belly patch is ~93% of the maximum chroma for this hue but only 53% of the maximum possible chroma for a pure hue of 0.75.